

THS







This is to certify that the

thesis entitled

# MORPHOLOGY VARIATIONS IN EXTRUSION OF POLYPROPYLENE/EP RUBBER BLENDS

presented by

Jonathan Michael Lopez

has been accepted towards fulfillment of the requirements for

M.S. degree in <u>Chemical</u> Engineering

Date 12/16/99

**O**-7639

MSU is an Affirmative Action/Equal Opportunity Institution

ajor professor

# PLACE IN RETURN BOX to remove this checkout from your record. TO AVOID FINES return on or before date due. MAY BE RECALLED with earlier due date if requested.

| DATE DUE                   | DATE DUE | DATE DUE |
|----------------------------|----------|----------|
| ốcî <sup>7</sup> 0 8 \$003 |          |          |
|                            |          |          |
|                            |          |          |
|                            |          |          |
|                            |          |          |
|                            |          |          |
|                            |          |          |
|                            |          |          |
|                            |          |          |
|                            |          | •        |

11/00 c:/CIRC/DateDue.p65-p.14

# MORPHOLOGY VARIATIONS IN EXTRUSION OF POLYPROPYLENE / EP RUBBER BLENDS

Ву

Jonathan Michael Lopez

# **A THESIS**

Submitted to
Michigan State University
in partial fulfillment of the requirements
for the degree of

**MASTER OF SCIENCE** 

Department of Chemical Engineering

#### **ABSTRACT**

# MORPHOLOGY VARIATIONS IN EXTRUSION OF POLYPROPYLENE / EP RUBBER BLENDS

By

# Jonathan Michael Lopez

This study investigates the morphology of two polymer blends containing polypropylene and one of two different grades of ethylene propylene (EP) rubber. Image analysis of SEM micrographs of the extrudates taken from different processing conditions reveals migration and varying degrees of stretching of the EP rubber drops from the wall to the center region of the die. The least volume fraction of the rubber phase was found to occur in the wall region, while the maximum degree of stretching was found to occur at the shear-free, center region of the capillary. At the center, the stretched rubber drops assumed a filament-like structure. Stretching that occurred in the wall region was found to be in the vorticity direction.

Greater apparent slip was found in the larger die diameters, where more migration was expected to occur. The amount of migration that occurs was explained in the terms of two competing fluxes, the flux due to viscosity variations and the flux due to collision. As viscosity increase with aspect ratio of the drops, the flux due to viscosity is expected to be significantly greater than the flux due to collisions in a small diameter die, where more stretching is expected to occur. This leads to a higher viscosity barrier in the core region for migration, so that less migration occurs in the small diameter dies.

In Loving Memory of Marina Gallardo Lopez

# **ACKNOWLEDGMENTS**

This research was supported by Montell Polyolefins and by the Michigan Materials and Processing Institute. I am pleased to acknowledge the assistance of Dr. Chi Chang Shu and Dr. M.D. Wolkowicz at Montell Polyolefins in identifying materials and preparing the blends for this study.

I would also like to express my sincere thanks to Dr. K. Jayaraman for not only helping me to define the problem in the early stages, but also for providing invaluable guidance during the course of this work. His energy and keen insight on the subject were inspirational and motivated me to perform quality research.

Lastly, I would like to thank my mother, father, brother, and my fellow colleagues for all of their support and patience. Special thanks go out to Darrell, Paul, and Sang-Yoon, who each made working at the office an enjoyable experience in their own special way. Thanks also go out to Guangda, Frank, Jason, Ben and Jen for their moral support and friendship.

# TABLE OF CONTENTS

| LIST OF TABLES                                  | vii  |
|---|------|
| LIST OF FIGURES                                 | viii |
| LIST OF SYMBOLS                                 | x    |
| CHAPTER 1                                       |      |
| INTRODUCTION                                    |      |
| 1.1 Entrance Pressure Effects                   |      |
| 1.2 Mooney Method for Determining Slip Velocity |      |
| 1.3 Apparent Slip                               |      |
| 1.4 Objectives                                  | 6    |
| CHAPTER 2                                       |      |
| PREVIOUS WORKS                                  | 7    |
| 2.1 Flow Lines on Injection Molded Parts        | 7    |
| 2.2 Classical Slip                              |      |
| 2.3 Apparent Wall Slip in Capillary Flow        | 9    |
| CHAPTER 3                                       |      |
| MORPHOLOGY OF POLYPROPYLENE / EP RUBBER BLENDS  | 12   |
| 3.1 Introduction                                |      |
| 3.2 Materials and Methods                       | 12   |
| 3.2.1 Experimental                              | 12   |
| 3.2.2 SEM analysis of morphology                | 13   |
| 3.3 Results and Discussion                      | 16   |
| 3.3.1 Cross-stream migration                    | 16   |
| 3.3.2 Stretching differential                   | 22   |
| 3.4 Conclusions                                 | 30   |
| CHAPTER 4                                       |      |
| RHEOLOGY OF POLYPROPYLENE / EP RUBBER BLENDS    | 32   |
| 4.1 Introduction                                | 32   |
| 4.2 Materials and Methods                       | 32   |
| 4.3 Phenomena in Capillary Flow Rheometry       |      |
| 4.3.1 Start-up pressure transients              |      |
| 4.3.2 Nonlinear Bagley plots                    |      |
| 4.3.3 Viscous heating effects                   |      |
| 4.4 Capillary Testing of Polypropylene 6323     |      |
| 4.4.1 Bagley corrections                        |      |
| 4.4.2 Mooney analysis                           |      |
| 4.5 Capillary Testing of 80/20 PP/EP Blends     |      |
| 4.5.1 Bagley corrections                        |      |

| 4.5.2 Mooney analysis                                 | 40 |
|---|----|
| 4.5.3 Recoverable strain in blends                    | 44 |
| 4.6 Conclusions                                       | 46 |
| CHAPTER 5 CONCLUSIONS AND RECOMMENDATIONS             | 47 |
| 5.1 Conclusions                                       | 47 |
| 5.2 Recommendations for Further Work                  |    |
| APPENDICES  |    |
| APPENDIX A. IMAGE ANALYSIS                            | 50 |
| A.1 Determination of Area Fraction                    |    |
| A.2 Determination of Average Aspect Ratio, \( \ell \) | 50 |
| APPENDIX B. DETERMINATION OF VOLUME FRACTION          |    |
| BIBLIOGRAPHY  | 55 |

# LIST OF TABLES

| Table 3.1 Diameters (in mm) of dies used for extruder and capillary rheometer  | . 13 |
|--|------|
| Table 3.2 Experimental conditions of CO-043 blend extrudates obtained for SEM analysis   | . 15 |
| Table 3.3 Range of distance (μm) of regions from center in Figure 3.3  | . 15 |
| <b>Table 3.4</b> Area fractions of CO-043 blend samples for regions indicated in Figure 3.3, L/D = 20 from micrographs perpendicular to flow |      |
| Table 3.5 Average aspect ratios and areas of rubber drops in regions 0-3 for sample E  | . 22 |
| Table 3.6 Capillary number in regions 0-3 for sample E   | . 24 |
| Table 3.7 Average aspect ratios and areas of rubber drops in wall region for samples A-F   | 28   |

# **LIST OF FIGURES**

| Figure 1.1 Schematic of a contraction in capillary flow.  | 3  |
|---|----|
| Figure 1.2 Mooney plot for a homogeneous polymer.   | 4  |
| Figure 1.3 Behavior of a system undergoing lubricated flow.   | 6  |
| <b>Figure 3.1</b> Micrographs of extrudate cores for (a) CO-043 blend, $\dot{\gamma}_{app} = 1,661 \text{ s}^{-1}$ and (b) MDE 251 blend, $\dot{\gamma}_{app} = 1,331 \text{ s}^{-1}$ at 200°C, D = 2 mm. |    |
| Figure 3.2 Drop size distributions in core for 80/20 blends at 200°C  | ۱4 |
| Figure 3.3 Cross-section of extrudate strand.   | 15 |
| <b>Figure 3.4</b> Perpendicular to flow micrographs of regions 1-3 for CO-043 blend extrudate $D = 1.5 \text{ mm}$ , $\dot{\gamma}_{app} = 2000 \text{ s}^{-1}$   |    |
| Figure 3.5 Flow plane micrographs of true center and regions 1-3 for CO-043 blend extrudate, D = 1.5 mm, $\dot{\gamma}_{app} = 2000 \text{ s}^{-1}$   | 19 |
| <b>Figure 3.6</b> Volume fractions from flow plane micrographs for CO-043 blend extrudate, $D = 1.5 \text{ mm}$ , $\dot{\gamma}_{app} = 2000 \text{ s}^{-1}$ , $t_{res} = 70 \text{ ms}$ .                |    |
| <b>Figure 3.7</b> Flow plane area distributions for regions 1-3 of CO-043 blend extrudate, $D = 1.5 \text{ mm}, \ \dot{\gamma}_{app} = 2000 \text{ s}^{-1}.$  | 22 |
| Figure 3.8 Plot of average aspect ratio for CO-043 blend, D = 1.5 mm, $\dot{\gamma}_{app} = 2000 \text{ s}^{-1}$  | 24 |
| Figure 3.9 Plot of viscosity ratio versus shear stress  | 26 |
| Figure 3.10 Viscosity ratio along radial position for CO-043 extrudate, D=1.5 mm, $\dot{\gamma}_{app} = 2000 \text{s}^{-1}$   |    |
| Figure 3.11 Plot of 2G' versus shear stress for components  | 27 |
| Figure 3.12 Micrographs of wall regions perpendicular to flow in extrudates A-D   | 29 |
| Figure 3.13 Micrographs of wall regions perpendicular to flow in extrudates E and F   | 30 |
| Figure 4.1 Bagley plot for 6323 PP for 1.0-mm diameter data at 200°C  | 35 |

| Figure 4.2 Bagley corrections for 6323 PP at 200°C                                    | 35 |
|---|----|
| Figure 4.3 Mooney plot for 6323 PP at 200°C, L/D=10                                   | 36 |
| Figure 4.4 Mooney plot for 6323 PP at 200°C, L/D=20                                   | 36 |
| Figure 4.5 Mooney plot for 6323 PP at 200°C, L/D=30.                                  | 37 |
| Figure 4.6 Slip velocities for 6323 PP at 200°C                                       | 37 |
| Figure 4.7 Bagley corrections for 80/20 6323 PP/MDE 251 at 200°C                      | 39 |
| Figure 4.8 Bagley corrections for 80/20 6323 PP/CO-043 at 200°C                       | 39 |
| Figure 4.9 Mean residence time versus wall shear stress for various die geometries    | 41 |
| Figure 4.10 Mooney plot for 80/20 6323 PP/MDE 251 at 200°C, L/D=20                    | 42 |
| Figure 4.11 Mooney plot for 80/20 6323 PP/CO-043 at 200°C, L/D=20                     | 42 |
| Figure 4.12 Schematic of dispersed phase concentration variation over radial position | 44 |
| Figure 4.13 Recoverable strain for 80/20 PP/EP blends at 200°C I /D=30 D=1 mm         | 45 |

#### LIST OF SYMBOLS

Ca : Capillary number.
D : Diameter of die, mm.
EP : Ethylene propylene.

EPDM: Ethylene propylene diene terpolymer.

HDPE: High density polyethylene.

K: Coefficient in power law model for viscosity, Pa · s.

 $\ell$ : Drop aspect ratio.

L/D : Length-to-diameter ratio.
MFR : Melt flow rate index.

M<sub>n</sub> : Number-average molecular weight.
 M<sub>w</sub> : Weight-average molecular weight.

n : Exponent in power law model for viscosity.

NMR : Nuclear magnetic resonance.

 $\Delta P$ : Pressure drop, MPa.

 $\Delta P_{en}$ : Pressure drop due to entrance effects, MPa.

PDI : Polydispersity index.

PMMA : Poly(methyl methacrylate).

PP : Polypropylene. PS : Polystyrene.

R : Radius of die, mm.

s : Reciprocal of power law model exponent, n.

SBR: Styrene butadiene rubber.
SEM: Scanning electron microscope.
SIM: Shear-induced migration

TEM : Transmission electron microscope.

TPO: Thermoplastic olefin. tres: Residence time, ms. slip velocity, m/s.

# **Greek Symbols**

δ : Thickness of lubricant layer.

\$\psi\$ : Volume fraction.

 $\dot{\gamma}_{app}$  : Apparent shear rate, s<sup>-1</sup>.

 $\eta$ : Shear viscosity, Pa · s.

 $\eta_c$ : Viscosity of core in lubricated flow model.

η<sub>1</sub>: Viscosity of lubricant layer in lubricated flow model

 $\tau_w$ : Wall shear stress, MPa.

### CHAPTER 1

#### INTRODUCTION

The occurrence of surface irregularities on injection molded parts has been the subject of much research in the field of polymer processing, particularly in the automotive industry where the demand for aesthetic quality can rank just as high as the demand for structural performance. Much debate has ensued as to what causes these surface defects, with wall slip, the loss of material adhesion between the polymer melt and the mold wall, being one of the leading theories. In order to better understand the mechanism by which these defects form, the flow behavior of these materials was investigated.

Polymers are generally known for their viscoelastic flow behavior, and they are used in structural applications which require some degree of stiffness. Rubbers, on the other hand, are somewhat more flexible and are generally tougher. Blending rubber with polymer thus yields a material which exhibits properties of both rubber and polymer. Polypropylene blended with ethylene propylene (EP) rubber falls within the class of materials known as thermoplastic olefins (TPOs). TPOs are of practical importance, since they are used extensively in the automotive industry for making bumpers and other car body parts.

A variety of rubbers, such as ethylene propylene diene terpolymer (EPDM) and styrene butadiene rubber (SBR), have been found to exhibit wall slip in capillary flow (Geiger, 1989; Mourniac et al., 1992; White *et al.*, 1991; Vinogradov, 1967). Wall slip has also been reported to occur in the flow of homogeneous polymers such as

polyethylene (Hatzikiriakos and Dealy, 1991, 1992). Slip effects may not be as pronounced in polypropylene systems because another phenomenon, viscous heating, may also be present to a considerable degree (Rosenbaum and Hatzikiriakos, 1997). In capillary flow, for example, the effect of viscous heating increases with increasing die diameter, while the occurrence of slip has just the opposite dependence on diameter.

Because slip has been shown to occur in both pure rubber and homopolymer systems, it is reasonable to assume that blends of polypropylene and EP rubber are prone to similar behavior in capillary flow.

### 1.1 Entrance Pressure Effects

The dependence of wall slip velocity on wall shear stress for a given melt can be determined from experiments using a capillary rheometer or with a lab-scale extruder. Pressure and flow rate data are used to calculate wall shear stress and apparent shear rate, respectively. Entrance effects of the polymer melt into the die are usually significant, and must be determined in order to calculate the true wall shear stress. In capillary flow, the magnitude of the entrance pressure effects increases with the contraction ratio, which is the ratio of the barrel diameter to the diameter of the die. A schematic of this contraction is shown in Figure 1.1.

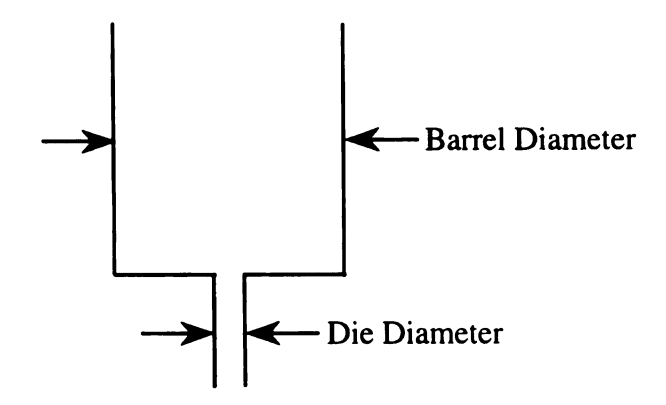


Figure 1.1 Schematic of a contraction in capillary flow.

The entrance pressure loss,  $\Delta P_{en}$ , is obtained by constructing a Bagley plot of pressure drop against length divided by diameter (L/D) with data obtained from dies of at least two different L/D ratios. The pressure drop,  $\Delta P$ , at a given apparent shear rate,  $\dot{\gamma}_{app}$ , will usually increase in direct proportion to increasing L/D ratios, such that the apparent shear rate curves will be linear. Extrapolation of these lines to an L/D of zero will yield  $\Delta P_{en}$ . The true wall shear stress,  $\tau_w$ , is then calculated by

$$\tau_{w} = \frac{\left(\Delta P - \Delta P_{en}\right)}{4L/D} \tag{1-1}$$

# 1.2 Mooney Method for Determining Slip Velocity

When slip flow occurs, the methods and corrections usually employed for determining rheological properties in capillary flow experiments must be modified considerably (Macosko, 1995; Hatzikiriakos *et al.*, 1992). The following relation may be derived for the apparent shear rate in isothermal flow of a power law fluid with wall slip in a capillary of radius R.

$$\dot{\gamma}_{app} = \frac{4u_s}{R} + \frac{4}{3+s} \left(\frac{\tau_w}{K}\right)^s \tag{1-2}$$

Here,  $u_s$  is the wall slip velocity,  $\tau_w$  is the wall shear stress, K is the coefficient of the power law viscosity model and s is the reciprocal of the power law exponent n. Above a critical wall shear stress, the flow curves (of wall shear stress vs. apparent shear rate) from dies of different diameters begin to diverge, exhibiting a diameter dependence.

Equation (1-2) forms the basis of Mooney plots, which are commonly used to determine slip velocity in a variety of homogeneous polymer systems. Mooney plots are plots of the apparent shear rate against 1/D at different fixed values of wall shear stress, for dies of different lengths and radii but the same L/D ratio (Figure 1.2). Extrapolation of these lines to 1/D = 0 yields the apparent shear rate that would be obtained at a given shear stress without wall slip. The slip velocity is determined by dividing the slope of the constant wall shear stress lines by 8. This procedure works well for several grades of polyethylene but not for polypropylene—presumably because viscous heating has a greater effect on the polypropylene melt viscosity (Kazatchkov *et al.*, 1995; Rosenbaum and Hatzikiriakos, 1997). An inherent failing of the Mooney technique is that it neglects the effects of temperature variations and of high pressure on viscosity, which can lead to inaccurate slip-velocity calculations. Another complication reported with rubber compounds is an additional dependence of slip velocity on die geometry (Mourniac *et al.*, 1992; Malkin *et. al.*, 1993).

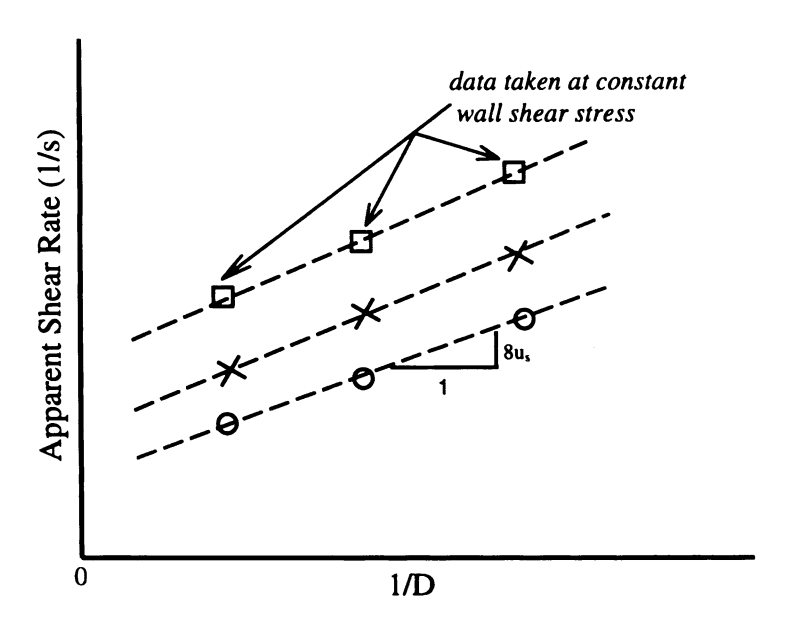


Figure 1.2 Mooney plot for a homogeneous polymer.

# 1.3 Apparent Slip

In multicomponent systems, the mechanism by which slip occurs can be somewhat more complicated, so much so that the Mooney procedure for inferring slip is no longer reliable. In these systems, a lubricant layer that can undergo classical slip, separate from the bulk flow, may form. This lubricant layer can form under one of three conditions: (1) migration of a lubricating or low viscosity component to the wall; (2) migration of a low surface energy component to the wall; or (3) inward migration of drops in flowing emulsions. As illustrated in Figure 1.3, this lubricant layer has some thickness  $\delta$  and an associated viscosity  $\eta_1$ . An example of the first case is the tube flow of water and oil systems. The second case was illustrated by Chan and Feng (1997) who

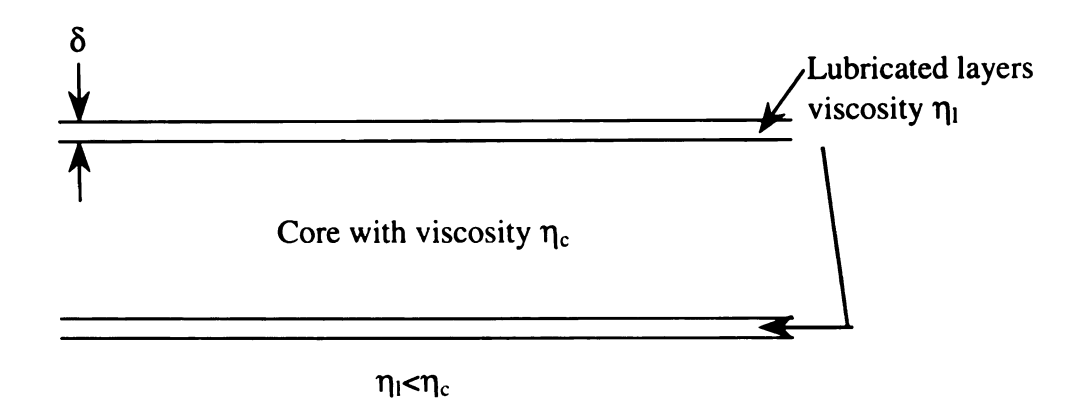


Figure 1.3 Behavior of a system undergoing lubricated flow.

performed a study with an HDPE blend mixed with Dynamar, a fluoroelastomer. They found that the Dynamar migrated and adhered to the wall, while the bulk melt detached from this wall layer. The third case is suspected to occur in polymer blends, with the rubber droplet phase migrating from the wall to the core region.

# 1.4 Objectives

To investigate the phenomenon of slip that may occur within these polymer blends, the main objectives of this study are:

- 1. To examine the morphology of the flowing blends under various extrusion conditions.
- 2. To relate trends in flow behavior to trends in morphology.

#### **CHAPTER 2**

### **PREVIOUS WORKS**

# 2.1 Flow Lines on Injection Molded Parts

Flow lines, the surface defects or irregularities on injection molded thermoplastic parts, are most prevalent when the material is a polymer blend, a rubber modified thermoplastic or a filled polymer (Han et al., 1996; Hobbs, 1996). These flow lines usually appear as alternating bands with different textures and degree of gloss, with the rough bands having a lower gloss and a duller appearance than the smooth bands (Hamada, 1996). Because the repeat patterns of the bands are different on the top and bottom surfaces of the part, these flow lines are suspected to stem from asymmetric instabilities that may develop in the melt flow (Chang, 1994; Hobbs, 1996). Hobbs (1996) conducted a study on the effect of gloss reducing additive particles on this phenomenon and found that although the width of the bands was greater than the particle size, the onset of these defects occurred at lower wall stresses, presumably due to the presence of the larger particles in the additive. These surface defects are thus assumed to be associated with slip flow just as, in extrusion operations, the occurrence of surface defects in the extrudate, such as "sharkskin" and "melt fracture," has been related to slip flow (Denn, 1990, 1992; El Kissi and Piau, 1990; Malkin et al., 1993).

# 2.2 Classical Slip

In solving the relevant equations for fluid flow, a common boundary condition that is assumed is the no-slip condition. For a majority of fluids, this assumption is usually true; however, in the processing of polymer melts, where the shear stress at the wall can become sufficiently high, this condition may not hold (Benbow, 1961). The high shear stress can induce slip flow, which refers to the loss of adhesion between the flowing melt and the wall. The onset of slip occurs at some critical wall shear stress,  $\tau_w$ , for a given polymeric material.

The techniques for quantifying slip were first developed by Mooney in 1931 (see Introduction). The underlying assumption in the Mooney technique is that the wall shear stress, slip velocity, temperature, and pressure gradient are constant along the length of the die and are independent of diameter.

Numerous authors have conducted slip studies of various homogeneous polymers to determine the mechanism by which slip occurs in these systems. Shidara and Denn (1993) found that polystyrene and polyethylene have very different slip characteristics. Polyethylene was found to exhibit wall slip, while polystyrene did not exhibit slip to an appreciable degree. Polydispersity also seems to have a major effect on the slip characteristics of the polymer, as polyethylene with a narrow molecular weight distribution is more likely to slip than broad molecular weight distribution polyethylene (Schowalter, 1988). Denn (1990) concluded that the more stretched the polymer chain, the more likely it is to slip.

# 2.3 Apparent Wall Slip in Capillary Flow

Apparent wall slip in the capillary flow of various polymer blends has been investigated extensively by numerous authors. The degree of slip evidenced in blends appears to depend on three interrelated factors, which may also account for the greater occurrence of flow lines with these systems. These are significant changes in the morphology of the melt flow, the associated blend rheology, and the different degrees of adherence of the components or phases to the mold walls.

Rofe and de Vargas et al. (1996) studied apparent wall slip effects in dilute xanthan solutions using nuclear magnetic resonance imaging (NMR) techniques and concluded that there were two main factors which correlated with the apparent slip in these systems. First, they found that the apparent slip velocity was related primarily to the wall shear stress as validated by their NMR and Mooney analysis experiments.

Second, results from gel permeation chromatography (GPC) strongly suggested that the degree of slip depended on the molecular weight of xanthan in solution. This was corroborated experimentally by recirculating the xanthan solution through a syringe pump. The pump destroyed a large portion of the high molecular weight xanthan and slip was no longer found to occur.

In suspensions, the mechanism by which apparent slip occurs can be somewhat more complicated. The particles in the suspension may migrate and establish concentration gradients, causing significant changes in rheology. Majors *et al.* (1989) made the first observation of shear-induced particle migration in circular conduits by using non-invasive NMR imaging techniques. The particles were found to migrate to regions of low-shear rate in the flow field, which caused an overall blunting of the

velocity profile. This blunting of the velocity profile has been corroborated by other authors (Karnis *et al.*, 1966; Arp and Mason, 1977; Sinton and Chow, 1991; Koh *et al.*, 1994).

Leighton and Acrivos (1987) proposed a mechanism for migration of suspensions of neutrally buoyant, mono-modal spherical particles in Newtonian fluids subjected to inhomogeneous shear flows. The key features of their mechanism are based on considering the effects of spatially varying viscosity and particle interaction frequency within the flow field. Utilizing the NMR measurements of the changing concentration and velocity profiles and the flux expressions proposed by Leighton and Acrivos, workers from MIT and Los Alamos derived a diffusion equation for the particulate phase (Phillips et al., 1992). The main assumption behind their shear-induced migration (SIM) model is that the suspension is a Newtonian fluid in which the viscosity is a function of the volume fraction of solids. An inherent limitation of this model is that it neglects the torques and pressure drops required to sustain flow. Graham et al. (1998) made the necessary modifications to the SIM model to account for the effects of non-local field variables, the curvature of the mean particle path and the concentration dependence of the particle interaction coefficient. The modified model was shown to provide very good agreement with experimental data by accurately predicting the migration of particles from the wall to the core. The model was even able to reproduce the plateau region in the concentration profile near the center as reported by Hampton et al. (1997) in his migration studies of pressure driven flow in circular conduits.

For emulsions containing non-rigid, deformable particles or drops, the morphology can be complicated further by the phenomena of drop break-up, coalescence,

and stretching. Bousmina and Muller (1998) studied the rheology and morphology of crosslinked polymethylmethacrylate rubber blends and found that the degree of stretch of the rubber drops varied going from the center to the wall region. Flow plane micrographs of the extrudate at various positions from the center of the capillary were obtained using a transmission electron microscope (TEM). The particles were found to become more stretched and aligned in the direction of the flow when going from the center to the outer radius. The alignment in the skin region of the extrudate was to found to result in a decrease in both viscosity and post-extrusion swell of the blends. Bousmina and Muller did not, however, report any radial concentration variations (i.e., no particle migration).

#### **CHAPTER 3**

# MORPHOLOGY OF POLYPROPYLENE / EP RUBBER BLENDS

#### 3.1 Introduction

The two-phase of morphology of a system containing viscoelastic drops dispersed in a viscoelastic matrix is suspected to have significant implications for the flow behavior. Break-up, migration, and stretching of the drops are likely to occur, which can drastically affect the melt rheology of these blends.

In order to gain a better understanding of how the flow behavior can be affected by these phenomena, the morphology of two blends containing 80/20 weight ratios of polypropylene and one of two different grades of EP rubber were examined with the aid of scanning electron microscopy (SEM).

#### 3.2 Materials and Methods

# 3.2.1 Experimental

Blends of polypropylene (MFR=11) and ethylene propylene (EP) rubbers—
EPSYN-MDE 251 (M<sub>w</sub>=285,000 and M<sub>w</sub>/M<sub>n</sub>=1.98) and Dutral CO-043 (M<sub>w</sub>=195,000 and M<sub>w</sub>/M<sub>n</sub>=5.24), were obtained from Montell Polyolefins, Inc. The PP was batch mixed, by Montell, with the EP in a Banbury mixer in 80/20 weight ratios at 200°C. The flow experiments were run on a ¾ in single-screw extruder attached to a Brabender plasticorder and also on a Kayeness 6052 DM Dynisco Capillary Rheometer. The dies used are listed in Table 3.1. The pressure transient was monitored to ensure that steady-state values of the pressure and flow rate were obtained.

Table 3.1 Diameters (in mm) of dies used for extruder and capillary rheometer.

|                     | L/D           |               |               |               |
|---------------------|---------------|---------------|---------------|---------------|
|                     | 10            | 15            | 20            | 30            |
| Extruder            |               | 1.0, 1.5, 2.0 | 1.0, 1.5, 2.0 | 1.0           |
| Capillary Rheometer | 0.5, 1.0, 1.5 |               | 0.5, 1.0, 1.5 | 0.5, 1.0, 1.5 |

# 3.2.2 SEM analysis of morphology

Preliminary SEM micrographs taken of the extrudate cores, revealed that the blend containing the CO-043 rubber had a finer dispersion of rubber drops than the blend containing MDE 251 (Figure 3.1). The drop size distribution was found to be much narrower in the CO-043 blend than in the MDE 251 blend (Figure 3.2). To facilitate the development of a predictive model, the CO-043 blend with the narrower distribution was chosen for further investigation.

To examine the changes in morphology in the melt flow, extrudate strands from the 0.5-, 1.0-, and 1.5-mm diameter dies of L/D=20 at shear rates of 500 and 2000 s<sup>-1</sup> were sent to Montell for scanning electron microscope (SEM) analyses. The six extrudate strands were labeled A-F as indicated in Table 3.2. Cross-sections of the strand were microtomed and the EP rubber was dissolved with methylcyclohexane, leaving visible voids in the PP matrix. Locations where micrographs were taken of the core-, mid-, and wall regions are indicated in Figure 3.3 and Table 3.3. Drop density and area fraction of the rubber phase in each of the micrographs were determined using Jandel Scientific's Sigma Scan Pro 3.0 image analysis software.

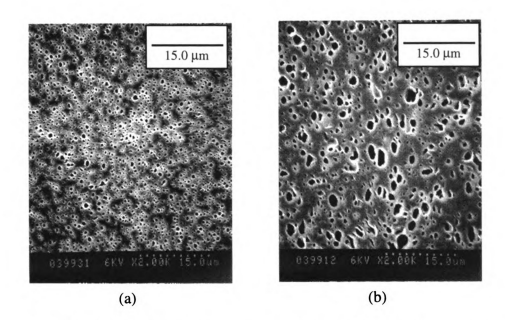


**Figure 3.1** Micrographs of extrudate cores for (a) CO-043 blend,  $\dot{\gamma}_{upp}=1.661~\text{s}^{-1}$  and (b) MDE 251 blend,  $\dot{\gamma}_{unp}=1.331~\text{s}^{-1}$  at 200°C, D = 2 mm.

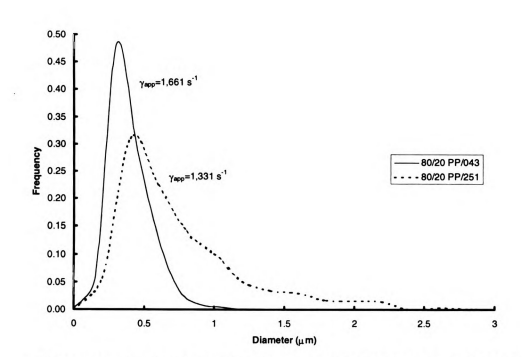


Figure 3.2 Drop size distributions in core for 80/20 PP/EP blends at 200°C.

**Table 3.2** Experimental conditions of CO-043 blend extrudates obtained for SEM analysis.

|           | Diameter, D* | Apparent Shear Rate, $\dot{\gamma}_{app}$ |  |  |
|-----------|--------------|---|--|--|
| Sample ID | (mm)         | (s <sup>-1</sup> )                        |  |  |
| A         | 0.5          | 2043.1                                    |  |  |
| В         | 0.5          | 486.45                                    |  |  |
| C         | 1.0          | 1994.45                                   |  |  |
| D         | 1.0          | 498.61                                    |  |  |
| E         | 1.5          | 1999.86                                   |  |  |
| F         | 1.5          | 500.87                                    |  |  |

<sup>\*</sup>Dies have L/D=20.

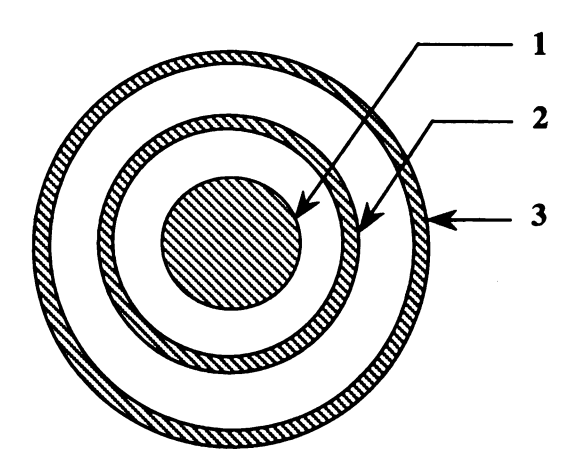


Figure 3.3 Cross-section of extrudate strand.

Table 3.3 Range of distance ( $\mu m$ ) of regions from center in Figure 3.3

| Extrudate Diameter (mm) | 1    | 2       | 3       |
|-------------------------|------|---------|---------|
| 0.5                     | <100 | 170-190 | 230-250 |
| 1                       | <200 | 300-350 | 470-500 |
| 1.5                     | <300 | 450-500 | 720-750 |

### 3.3 Results and Discussion

# 3.3.1 Cross-stream migration

Micrographs of regions 1-3 for the 1.5-mm diameter sample at an apparent shear rate of 2000 s<sup>-1</sup> are shown in Figure 3.4 for the CO-043 blend. Flow plane micrographs of sample E were also taken and are shown in Figure 3.5. (It should be noted that a true center micrograph was obtained in the flow plane region, while region 1 in the perpendicular to flow micrograph was confirmed to be ~250 μm from the true center.)

Because of the stretching that occurs in the flow plane, the area fractions in the perpendicular to flow view are biased. (For a detailed discussion on how the area fraction was calculated, see Appendix A). As seen in Table 3.4, the radial variations of the area fraction differ from one extrudate to another. For extrudates A, B, and D the greatest concentration of rubber appears to be in region 2, the region between the core and the wall; for extrudates C and F, there appears to be a gradient in the rubber concentration with the maximum being at the core; and for extrudate E, the concentration gradient is in the opposite direction, with the maximum concentration of rubber at the wall. The area fraction at the center of the extrudates (region 1) appears to decrease with die diameter, suggesting that stretching in the flow plane seems to increase with decreasing die diameter.

The radial variation of the area fraction of the rubber in each of the samples provides strong evidence of migration. As the stretching appears to be primarily in the direction of flow, the volume fractions for extrudate E were determined based on the flow plane area fractions measured in each region. (See Appendix B for a discussion of how the volume fraction was determined.) As seen in Figure 3.6, the volume fraction of the

**Table 3.4** Area fractions of CO-043 blend samples for regions indicated in Figure 3.3, L/D = 20, from micrographs perpendicular to flow.

|           | D    | $\dot{\gamma}_{app}$ | Area Fraction of Drops in Region |       |        |  |
|-----------|------|----------------------|----------------------------------|-------|--------|--|
| Sample ID | (mm) | (s <sup>-1</sup> )   | 1                                | 2     | 3      |  |
| Α         | 0.5  | 2043.1               | 0.0916                           | 0.110 | 0.0830 |  |
| В         | 0.5  | 486.45               | 0.0911                           | 0.144 | 0.0863 |  |
| C         | 1.0  | 1994.45              | 0.118                            | 0.112 | 0.0869 |  |
| D         | 1.0  | 498.61               | 0.135                            | 0.155 | 0.136  |  |
| E         | 1.5  | 1999.86              | 0.132                            | 0.140 | 0.151  |  |
| F         | 1.5  | 500.87               | 0.177                            | 0.130 | 0.0835 |  |

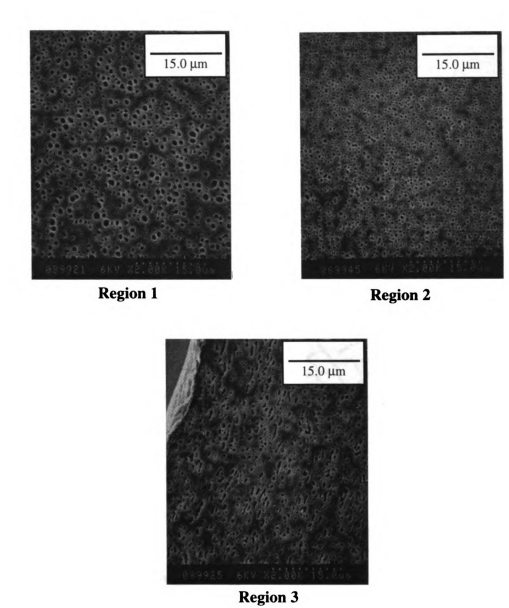


**Figure 3.4** Perpendicular to flow micrographs of regions 1-3 for CO-043 blend extrudate, D = 1.5 mm,  $\dot{\gamma}_{app}$  = 2000 s<sup>-1</sup>.

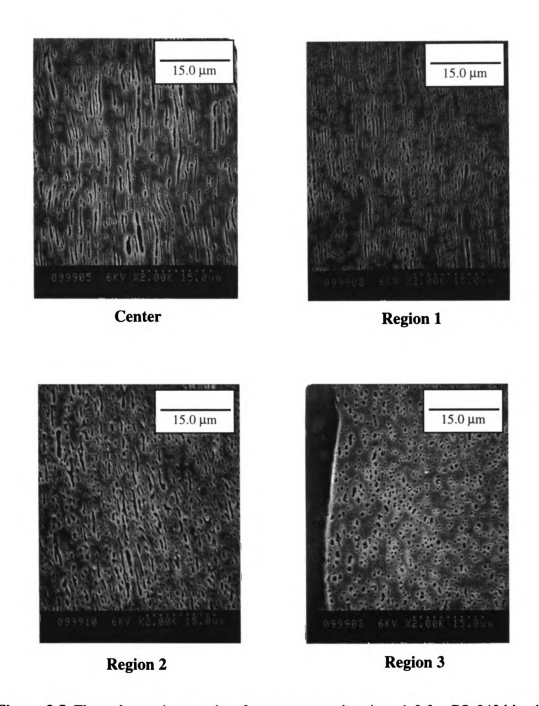


Figure 3.5 Flow plane micrographs of true center and regions 1-3 for CO-043 blend extrudate, D=1.5 mm,  $\dot{\gamma}_{upp}=2000~s^{-1}.$ 

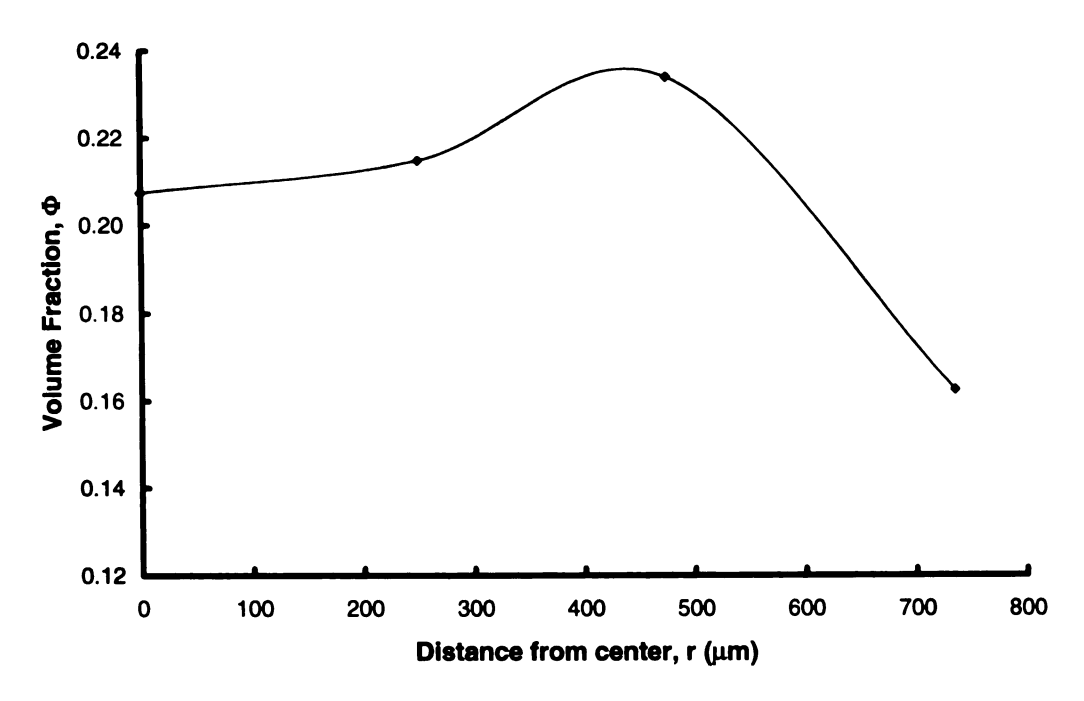


Figure 3.6 Volume fractions from flow plane micrographs for CO-043 blend extrudate, D = 1.5 mm,  $\dot{\gamma}_{app} = 2000 \text{ s}^{-1}$ ,  $t_{res} = 70 \text{ ms}$ .

rubber seems to reach a maximum in region 2, which seems to concur with the trends in the perpendicular to flow view for all of the other samples, except C and F.

One would expect that the maximum concentration of rubber be at the core and not in the region between the center and the wall, so the following explanation is offered. It has been shown that the dispersion of rigid, spherical particles in suspensions can have a major effect on the overall flow characteristics of the system, causing such effects as the blunting of the velocity profile (Sinton and Chow, 1991; Koh  $et\ al.$ , 1994) and the reduction of extrudate swell (Newman and Trementozzi, 1965). It has also been found that the length at which the flow becomes fully developed depends on the bulk volume fraction of the dispersed phase and the ratio of the average drop size to the radius of the die (a/R). Hampton  $et\ al.$  (1997) concluded from their study on the demixing of neutrally buoyant suspensions of spheres that as both the bulk volume fraction and a/R decreases,

the entrance length required for fully developed flow increases. For suspensions of volume fraction of 0.2 and a/R = 0.0256, they found that an entrance length on the order of  $10^3$  diameters was required for fully developed flow.

In the CO-043 blend, where the bulk volume fraction is about 0.22 and the average particle size is roughly 1  $\mu$ m, yielding a maximum value of a/R on the order of  $10^{-3}$ , the flow can not be assumed to be fully developed. The situation is further complicated by the fact that the dispersed phase consists of deformable, viscoelastic drops and not rigid spherical particles. Caution thus must be exercised when interpreting the concentration profiles (Figure 3.6) obtained from the capillary rheometry of these blends, as these profiles are not representative of what occurs at steady-state.

Cross-stream migration of the rubber drops is further corroborated by the differential in the size of the drops in each of the regions. As seen in Figure 3.7, the area distribution in the parallel to flow view for the wall layer (Region 3) of sample E is shifted towards smaller-sized drops in comparison to the area distributions in regions 1 and 2. The volume-averaged drop size in region 3 of the flow plane was found to be smaller than the sizes determined in the other regions (Table 3.5). This suggests the inward migration of the larger size drops from the wall to the core, since the particles are moving away from the region of greatest shear stress (i.e., the wall).

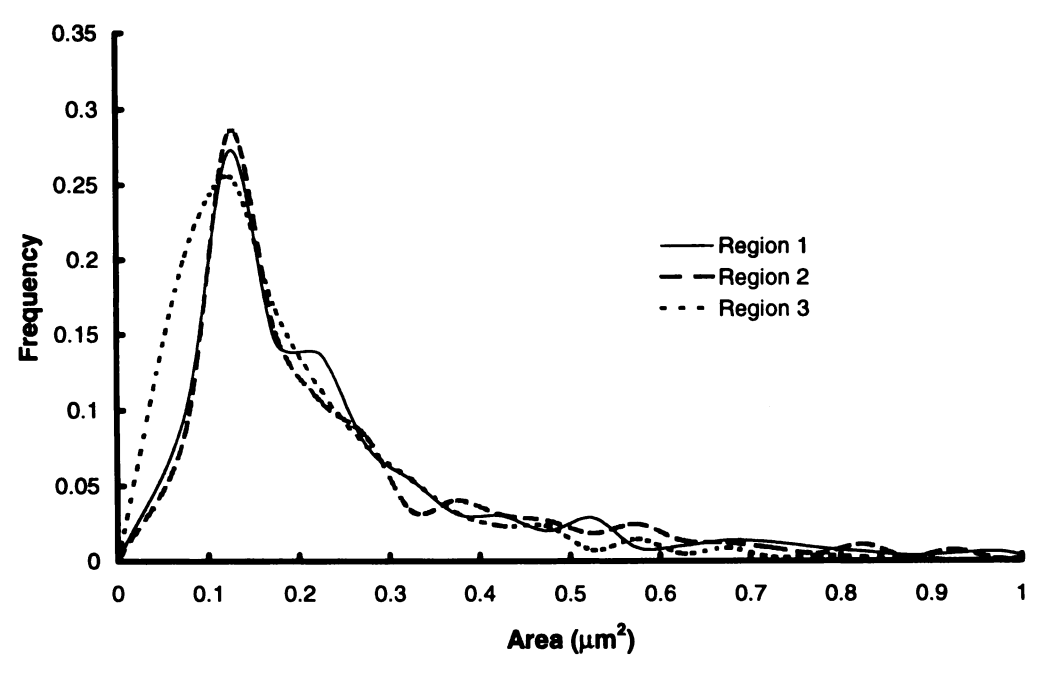


**Figure 3.7** Flow plane area distributions for regions 1-3 of CO-043 blend extrudate, D = 1.5 mm,  $\dot{\gamma}_{app} = 2000 \text{ s}^{-1}$ .

Table 3.5 Average aspect ratios and areas of rubber drops in regions 0-3 for sample E.

|                   | Perp | Regio<br>pendicular |       | View  |       | Regio<br>Flow Pla |       |       |
|-------------------|------|---------------------|-------|-------|-------|-------------------|-------|-------|
| Quantity          | 0    | 1                   | 2     | 3     | 0     | 1                 | 2     | 3     |
| $\ell_{v}$        | -    | 1.51                | 1.56  | 2.33  | 8.41  | 6.27              | 3.38  | 1.62  |
| $\ell_n$          | -    | 1.42                | 1.48  | 1.88  | 4.59  | 3.05              | 2.29  | 1.50  |
| _ℓ <sub>PDI</sub> | -    | 1.06                | 1.06  | 1.24  | 1.83  | 2.06              | 1.47  | 1.08  |
| $A_v (\mu m^2)$   | -    | 0.435               | 0.149 | 0.452 | 1.90  | 0.630             | 0.917 | 0.326 |
| $A_n (\mu m^2)$   | -    | 0.212               | 0.099 | 0.237 | 0.632 | 0.242             | 0.282 | 0.163 |
| A <sub>PDI</sub>  | -    | 2.05                | 1.50  | 1.91  | 3.00  | 2.60              | 3.25  | 2.00  |

# 3.3.2 Stretching differential

A number of studies have been conducted on the deformation of viscoelastic drops in a viscoelastic matrix (Mighri et. al, 1998; Levitt et. al, 1999; Hobbie and Migler, 1999). Bousmina and Muller (1996) found that in the flow plane view of PMMA/rubber

blend extrudates, the rubber phase become more stretched and oriented near the core the wall. This is in stark contrast with what is observed in the flow plane views for sample E. As seen in Figure 3.5, the drops become more oriented and stretched in the core, where they assume a filament-like structure (Figure 3.5). In the wall region, the stretching yields ellipsoidal structures that are oriented in the vorticity direction, which is perpendicular to the flow (Figure 3.4). To quantify the degree of stretch occurring in each of the regions, we define aspect ratio, which is the ratio of the length of drop to the diameter of the drop, or

Aspect Ratio = 
$$\ell = \frac{\text{Length of Drop}}{\text{Diameter of Drop}}$$
 (3-1)

A plot of the aspect ratio of the drops in the different regions (Figure 3.8) for both the perpendicular and flow-plane views shows that the maximum stretching is found in the outer skin region for the perpendicular to flow; however, in the flow plane, the stretching is the greatest at the center.

It is useful at this point to define the capillary number, which is a dimensionless ratio between the viscous stresses exerted on the drop by the external flow field and the interfacial stresses that tend to restore the drop to a spherical shape. This is given as

$$Ca = \frac{\tau_w(r/R)}{\Gamma/a}$$
 (3-2)

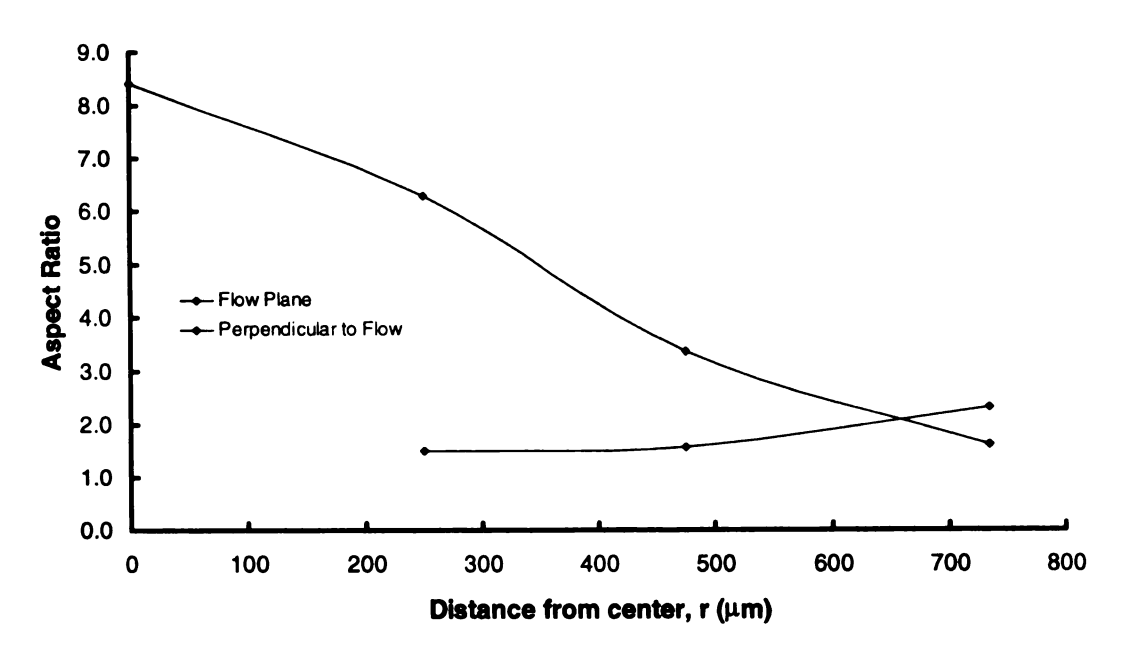


**Figure 3.8** Plot of average aspect ratio for CO-043 blend, D = 1.5 mm,  $\dot{\gamma}_{app} = 2000 \text{ s}^{-1}$ .

where Ca is the capillary number,  $\tau_w$  is the wall shear stress, r is the radial position, R is die radius, a is the average drop size, and  $\Gamma$  is the interfacial tension. For Ca<1, the drops are prone to retain their shape, while for Ca>>1 the drops tend to deform or stretch. Data obtained from the supplier of the rubber shows that  $\Gamma$  ranges from 0.5-1.0 mN/m. As seen in Table 3.6, the capillary number is considerably greater than one in all regions.

**Table 3.6** Capillary number in regions 0-3 for sample E.

|                  | Center | 1  | 2  | 3  |
|------------------|--------|----|----|----|
| Capillary Number | 0      | 42 | 95 | 88 |

Table 3.5 summarizes the weighted- and number-averages of the aspect ratio and area of each region and also gives the dispersity indexes (PDI) of the distributions, where

PDI is defined generically here as the ratio of a weighted-average quantity to a number-average quantity. The drops in region 2 of the flow plane were not only considerably larger than the drops in regions 1 and 3, but they also had the greatest variation in size with a PDI of 3.25. Consequently, for the corresponding perpendicular to flow view, the drops in region 2 were found to be the smallest when compared to the drop sizes in regions 1 and 3, which suggests that the majority of the stretching in this region occurred in the flow plane.

The stretching at the center, shear-free zone of the extrudate warrants further explanation. A plot of the viscosity ratio of the EP rubber phase to the polypropylene matrix versus shear stress shows that the rubber phase has a consistently greater viscosity than the polypropylene for a wide range of shear stresses, with the MDE 251 having a higher viscosity ratio than the CO-043 (Figure 3.9). Plotting the viscosity ratio versus radial position for extrudate E (Figure 3.10) reveals that the viscosity ranges from 1.8 at the center to 30 near the wall. A number of studies conducted on drop break-up in purely Newtonian systems in simple shear flow (Grace, 1982; Torza *et al.*, 1972; Karam and Bellinger, 1968) have shown that drop break-up occurs in these systems at viscosity ratios of less than 4. At the center of extrudate E, however, there is no evidence of substantial drop break-up, but stretching is evident.

At low shear stresses, the normal stress difference can be approximated by two times the storage modulus  $G'(\omega)$ . A plot of 2G' versus shear stress (Figure 3.11) shows that both rubbers have a consistently lower normal stress than the 6323 PP. Despite the low viscosity ratio of the CO-043 rubber at the center of the extrudate, the lower normal

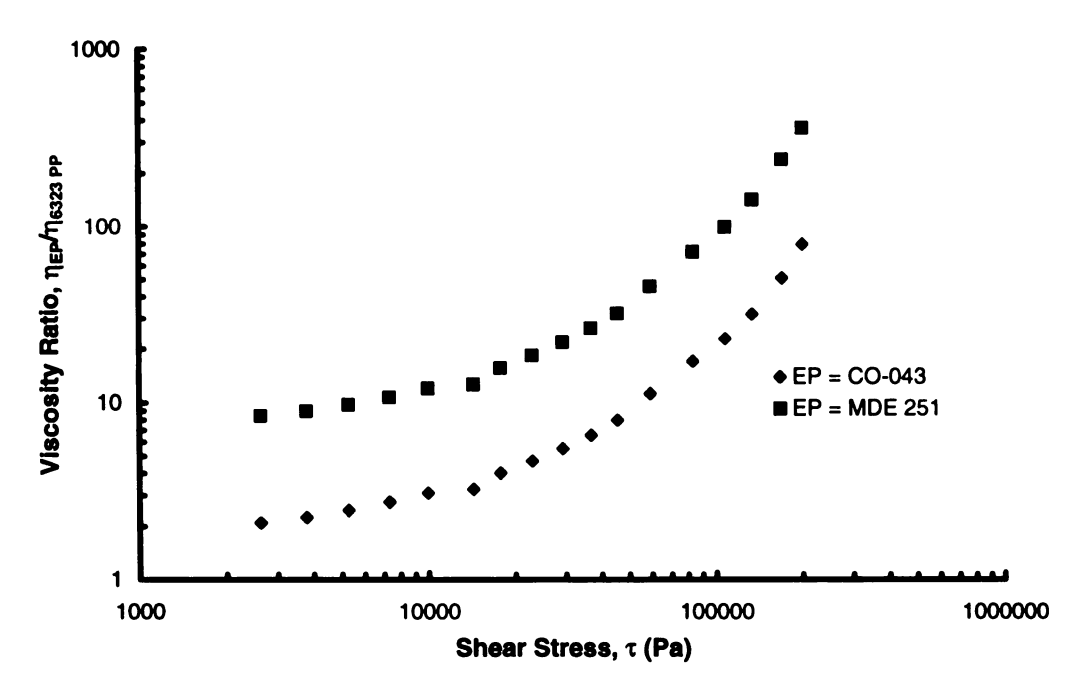
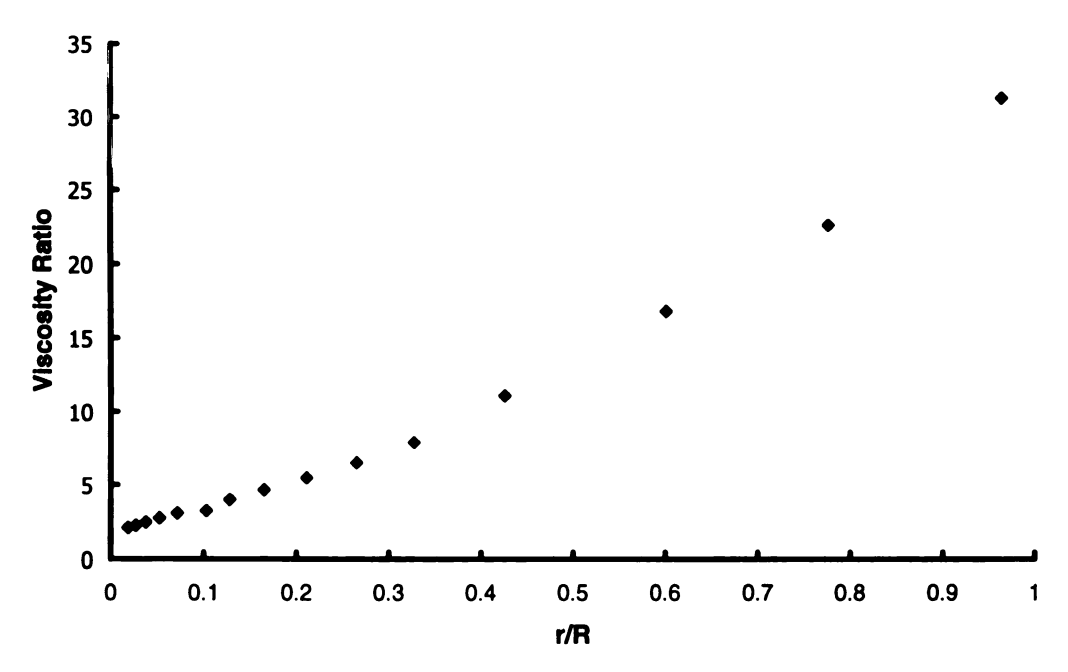


Figure 3.9 Plot of viscosity ratio versus shear stress.



**Figure 3.10** Viscosity ratio along radial position for CO-043 extrudate, D=1.5 mm,  $\dot{\gamma}_{app} = 2000 \, \text{s}^{-1}$ .

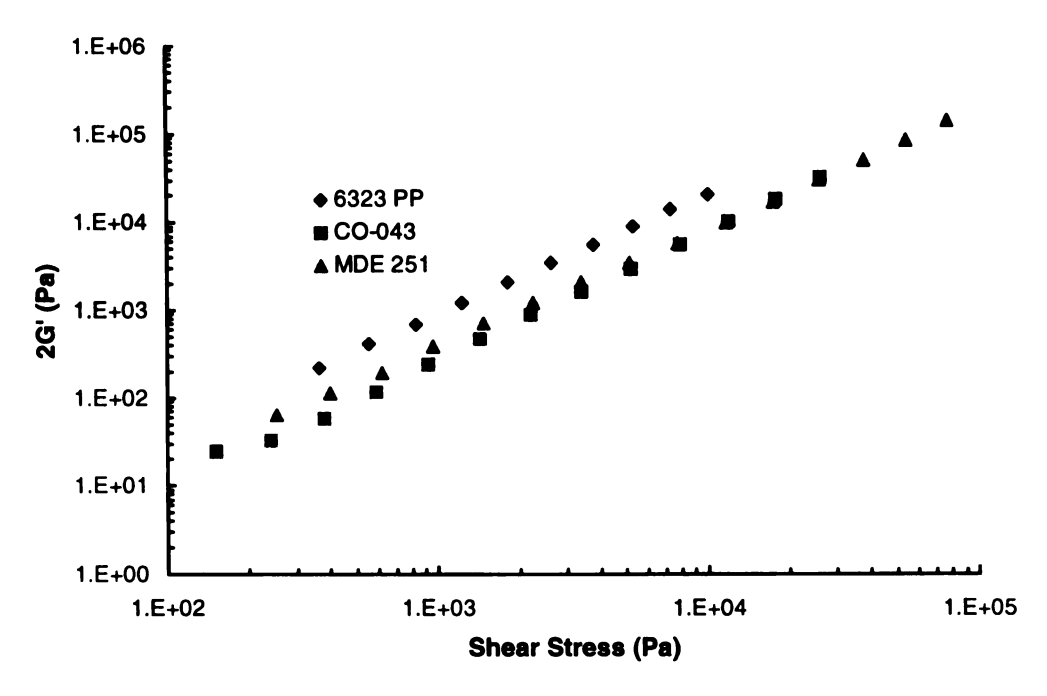


Figure 3.11 Plot of 2G' versus shear stress for components.

stress of the rubber as compared to that of the PP matrix, makes the rubber drops prone to stretching in the direction of the flow.

The average aspect ratios and areas for the rubber drops in the wall regions for samples A-F are listed in Table 3.7. The most obvious trend is that the average area or size of the drops tend to increase with increasing diameter at a given shear rate. The PDI of the area distributions appears to be both a function of diameter and shear rate. For a shear rate of 2000 s<sup>-1</sup>, the PDIs of the area distributions seems to remain constant regardless of diameter; however, at the lower shear rate, the 0.5-mm diameter was found to have a narrower distribution of drop sizes than what was observed at the larger diameters. The drop aspect ratio, as expected, was shown to increase with shear rate.

Another feature that was prominent in the wall region of each the extrudates was the elongation of the rubber drops in the vorticity direction, which is perpendicular to the

**Table 3.7** Average aspect ratios and areas of rubber drops in wall region for samples A-F.

|                    | $\dot{\gamma}_{app} = 500 \mathrm{s}^{-1}$ |                    |        | $\dot{\gamma}_{app} = 2000 \mathrm{s}^{-1}$ |                    |        |
|--------------------|--|--------------------|--------|---|--------------------|--------|
| Quantity           | 0.5 mm                                     | 1.0 mm<br>Diameter | 1.5 mm | 0.5 mm                                      | 1.0 mm<br>Diameter | 1.5 mm |
| $\tau_w$ (MPa)     | 0.098                                      | 0.099              | 0.097  | 0.165                                       | 0.157              | 0.152  |
| $\ell_{\nu}$       | 1.84                                       | 2.01               | 2.18   | 2.50  | 2.22               | 2.33   |
| $\ell_n$           | 1.62                                       | 1.75               | 1.86   | 2.03  | 1.83               | 1.88   |
| $\ell_{	ext{PDI}}$ | 1.14                                       | 1.15               | 1.17   | 1.23  | 1.22               | 1.24   |
| $A_v (\mu m^2)$    | 0.141                                      | 0.376              | 0.570  | 0.149                                       | 0.157              | 0.452  |
| $A_n (\mu m^2)$    | 0.085                                      | 0.180              | 0.275  | 0.076                                       | 0.082              | 0.237  |
| A <sub>PDI</sub>   | 1.66                                       | 2.09               | 2.07   | 1.96  | 1.91               | 1.91   |

flow (Figures 3.12-3.13) This phenomenon was reported by Hobbie and Migler (1999) in their study of shear- induced deformation of dilute emulsions of viscoelastic polymer melts and found to occur at some critical shear stress where the normal stress of the dispersed phase and of the matrix matched. Using 2G' as an estimate of the normal stress, extrapolation of the curves for PP and the two rubbers was found to overpredict the wall shear stress at which vorticity elongation occurs in these blends. This suggests that 2G' is a poor estimate of the normal stress at high shear stresses.



Sample A,  $\dot{\gamma}_{app} = 2043 \text{ s}^{-1}$ , D=0.5 mm



Sample B,  $\dot{\gamma}_{app} = 486 \text{ s}^{-1}$ , D=0.5 mm

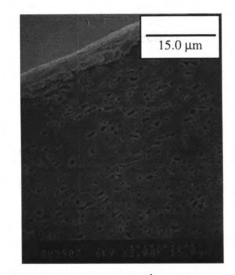


Sample C,  $\dot{\gamma}_{app} = 1994 \text{ s}^{-1}$ , D=1.0 mm Sample D,  $\dot{\gamma}_{app} = 499 \text{ s}^{-1}$ , D=1.0 mm



Figure 3.12 Micrographs of wall regions perpendicular to flow in extrudates A-D.





Sample E,  $\dot{\gamma}_{app} = 2000 \text{ s}^{-1}$ , D=1.5 mm

Sample F,  $\dot{\gamma}_{app} = 500s^{-1}$ , D=1.5 mm

Figure 3.13 Micrographs of wall regions perpendicular to flow in extrudates E and F.

#### 3.4 Conclusions

This study has shown that in emulsions of EP rubber dispersed in a PP matrix, the rubber drops undergo both migration and stretching along different directions as one moves from the center of the capillary to the outer radius. From the flow plane micrographs of the 1.5-mm diameter extrudate taken at an apparent shear rate of 2000 s<sup>-1</sup>, the maximum concentration of rubber drops was found to be in the region between the center and the wall; however, caution must be exercised when interpreting these results as it was shown that the flow was not fully developed. Stretching was found to yield filament-like structures in the flow plane view at the center or shear-free zone of the extrudate, while the maximum amount of stretching in the perpendicular to flow view seemed to occur in the wall region, where the drops assume an ellipsoidal-like structure.

The sizes of the drops in the wall region were found to increase with die diameter and with shear rate and elongation of the drops took place in the vorticity direction.

A reasonable estimate of the volume fractions could not be obtained for the other extrudates, since stretching may also be occurring in the flow plane of these samples, resulting in a distorted view of the true drop size in the perpendicular to flow view.

Further work would entail obtaining a more detailed picture of the 3-D structure of the rubber drops to gain a better estimate of volume fraction.

#### **CHAPTER 4**

#### RHEOLOGY OF POLYPROPYLENE / EP RUBBER BLENDS

#### 4.1 Introduction

In this chapter, the rheology of the blends is discussed in light of the information gained from the morphology study. Specifically, a connection is made between the phenomena of drop migration and deformation to apparent slip, viscosity and extrudate swell. Neat polypropylene is discussed first as a reference case.

#### 4.2 Materials and Methods

Neat polypropylene (MFR=11) and blends of polypropylene and ethylene propylene (EP) rubbers—EPSYN-MDE 251 ( $M_w$ =285,000 and  $M_w/M_n$ =1.98) and Dutral CO-043 ( $M_w$ =195,000 and  $M_w/M_n$ =5.24), were obtained from Montell Polyolefins, Inc. The PP was batch mixed with the EP in a Banbury mixer in 80/20 weight ratios at 200°C. The flow experiments were run on a Kayeness 6052 DM Dynisco capillary rheometer. The dies used are listed in Table 3.1.

### 4.3 Phenomena in Capillary Flow Rheometry

# 4.3.1 Start-up pressure transients

Hatzikiriakos and Dealy (1994) performed a study on the start-up pressure transients in the capillary rheometry of various polyethylenes and found that the time required to achieve a steady pressure reading at constant piston speed, also known as the

"rise time," increases with L/D and the amount of polymer in the reservoir and decreases with diameter and piston speed.

In all of the flow tests performed in this study, the pressure transient was monitored to ensure that data obtained was at steady state.

### 4.3.2. Nonlinear Bagley plots

The entrance pressure effects were determined using the Bagley method as described in Section 1.1. Curvature may occur in the Bagley plot if the viscosity of the system has a significant pressure dependency (Laun, 1983; Laun and Schuch, 1990), or if the slip velocity is strongly affected by pressure (Hatzikriakos and Dealy, 1992). In either case, care must be taken in extrapolating the Bagley plot curves to obtain the proper ends corrections.

### 4.3.3 Viscous heating effects

Another phenomenon than can occur in the capillary flow of polymer melts is viscous heating effects. When a viscous material is deformed in a flow field, some of the work of deformation is converted into thermal energy, which can cause a substantial rise in temperature within the flow. The high viscosities and low thermal conductivities of polymers make them especially prone to viscous dissipation. Hatzikiriakos and Dealy (1997) concluded from their numerical analyses of capillary flow undergoing slip and viscous heating effects, that viscous heating increases with apparent shear rate and die diameter. Since the Mooney technique neglects the effects of temperature and pressure,

data obtained from systems that undergo a significant amount of viscous dissipation appear as curved lines on the Mooney plot. Slip effects can therefore be masked by viscous heating in eliminating the diameter-dependency of the flow curves (Katzatchkov and Hatzikiriakos, 1997).

# 4.4 Capillary Testing of Polypropylene 6323

## 4.4.1 Bagley corrections

The Bagley plots for all L/D's were slightly curved especially at high shear rates, indicating that the slip velocity has some dependence on pressure (Hatzikiriakos and Dealy, 1992). The ends correction  $\Delta P_{en}$  was thus estimated by a second-order polynomial extrapolation of the data to the y-axis (Figure 4.1 shows the Bagley plot for the 1.0-mm diameter data). A plot of the Bagley corrections (Figure 4.2) shows that the  $\Delta P_{en}$  are a diameter dependent, which is due to the different contraction ratios for each die diameter.

#### 4.4.2 Mooney analysis

Plots of the corrected data on Mooney coordinates are shown in Figures 4.3-4.5. Estimates of the slip velocity as a function of wall shear stress were determined from the 1.5- and 1.0-mm diameter data (Figure 4.6). Slip velocity was found to decrease with increasing L/D, a trend also reported to occur with high density polyethylenes (HDPEs) by Hatzikiriakos and Dealy (1992). Since viscous heating has also been determined to occur in the capillary flow of polypropylene, some of the reduction in the "apparent" slip velocity may be due to the increasing effect of viscous heating with increasing L/D.

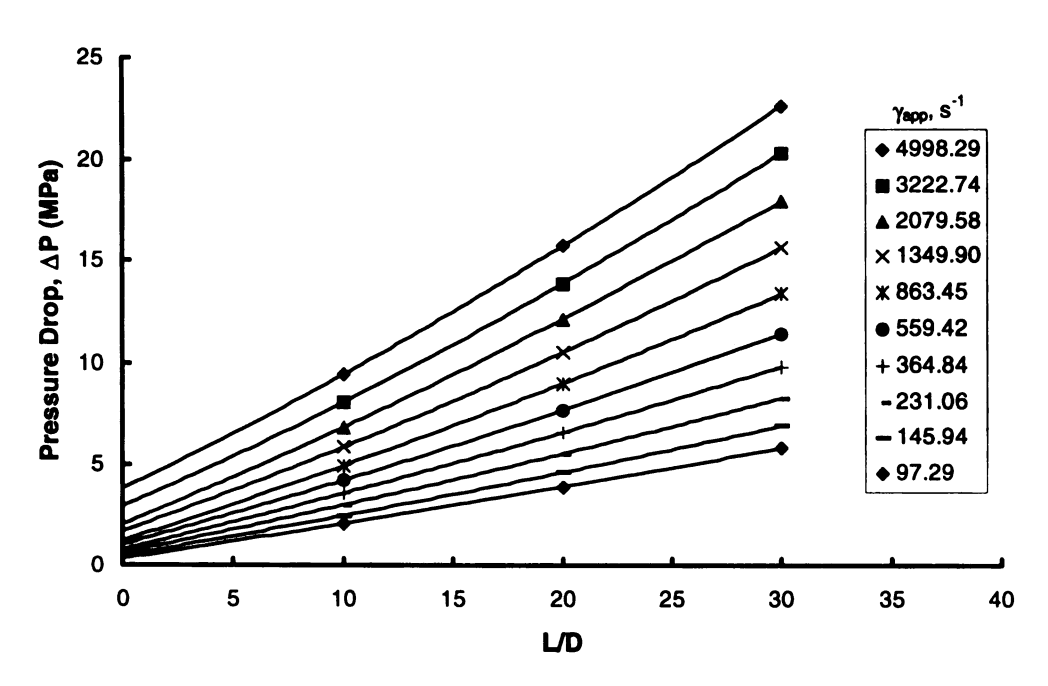


Figure 4.1 Bagley plot for 6323 PP for 1.0-mm diameter dies at 200°C.

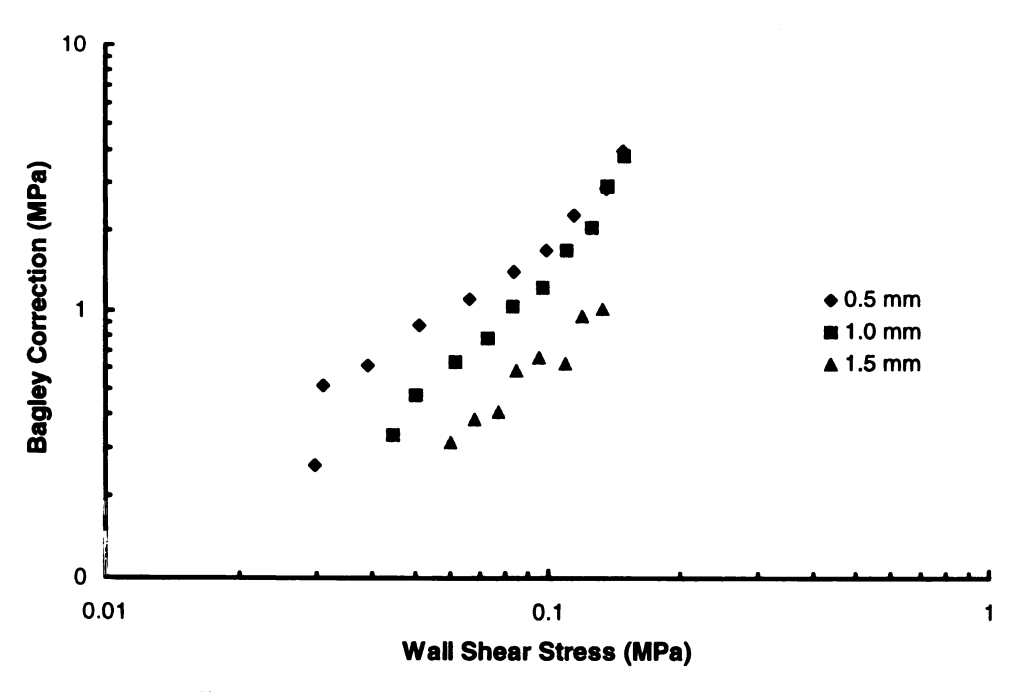


Figure 4.2 Bagley corrections for 6323 PP at 200°C.

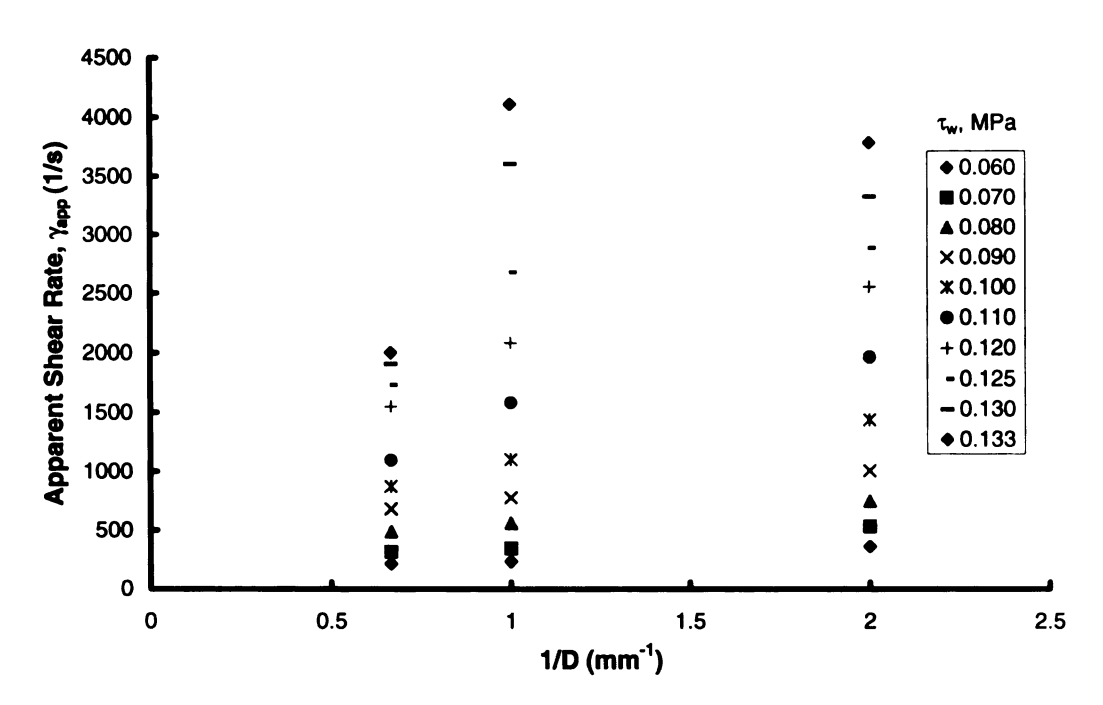


Figure 4.3 Mooney plot for 6323 PP at 200°C, L/D = 10.

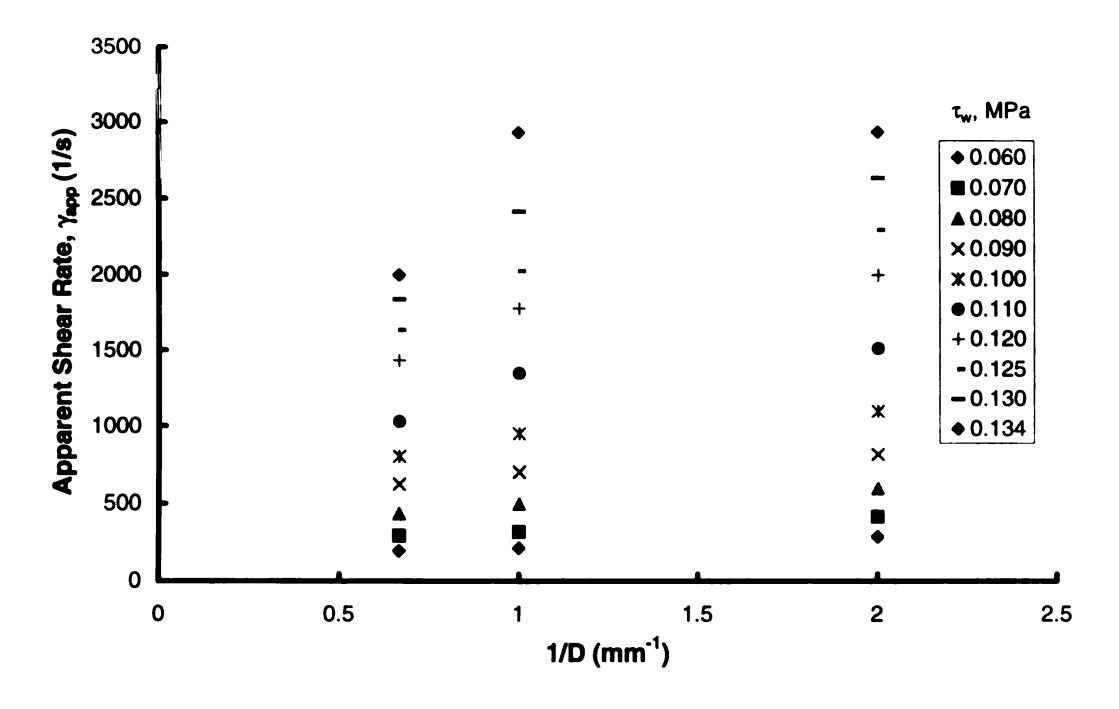


Figure 4.4 Mooney plot for 6323 PP at 200°C, L/D =20.

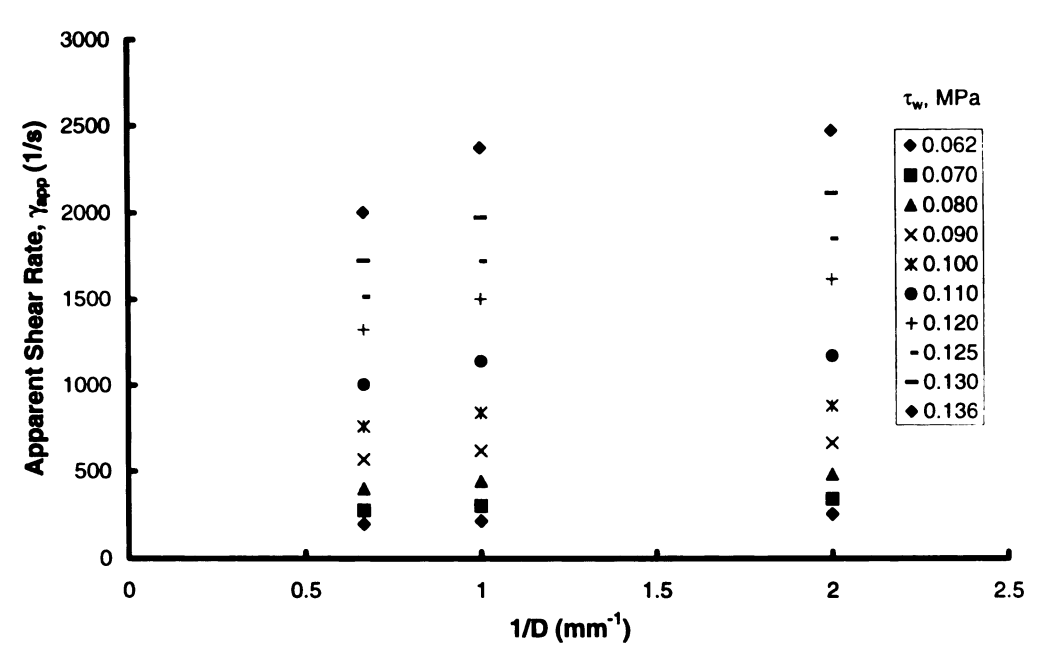


Figure 4.5 Mooney plot for 6323 PP at  $200^{\circ}$ C, L/D =30.

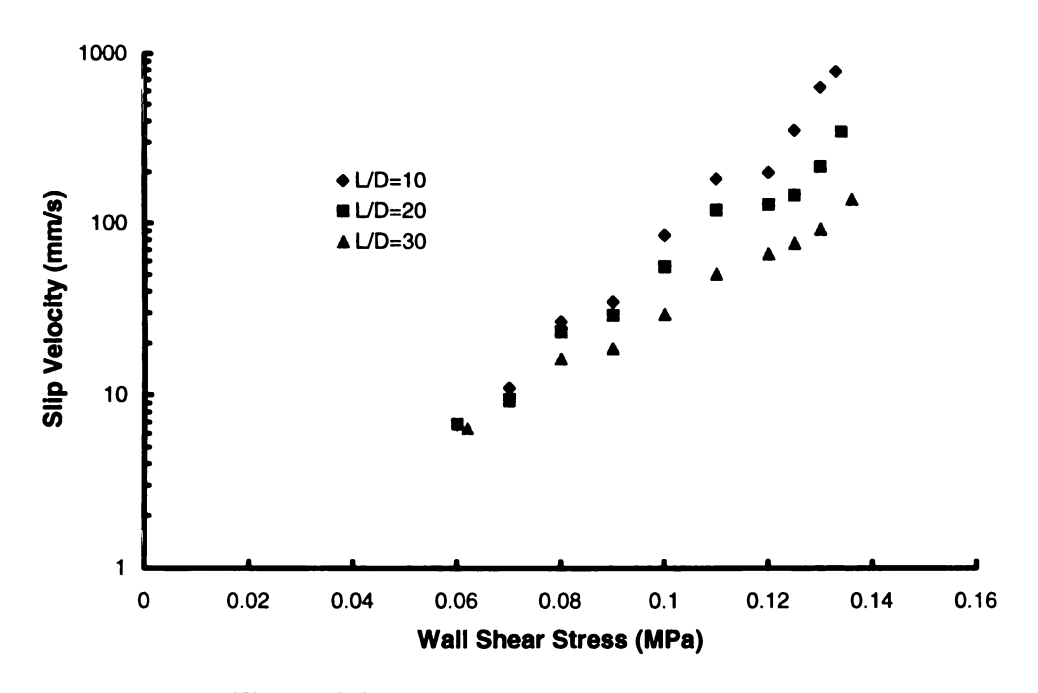


Figure 4.6 Slip velocities for 6323 PP at 200°C.

# 4.5 Capillary Testing of 80/20 PP/EP Blends

### 4.5.1 Bagley corrections

The Bagley plots for both blends at all three diameters were curved, so that a second-order polynomial fit was used to obtain  $\Delta P_{en}$ . A plot of  $\Delta P_{en}$  versus wall shear stress shows that  $\Delta P_{en}$  for the MDE 251 blend has a similar dependence on contraction ratio as does the neat PP (Figure 4.7), with the small dies (large contraction ratio) having a greater Bagley correction than the large dies (small contraction ratio).

The plot of  $\Delta P_{en}$  versus wall shear stress for the CO-043 blend, however, does not show any consistent trends with contraction ratio. The effects of morphology are believed to have a significant effect on the entrance pressure for this particular system. Han *et al.* (1995) concluded in his study of polystyrene (PS)/poly(methyl methacrylate) (PMMA) blends, that because of the significant deformation of the dispersed PMMA droplets as they entered the entrance region of the die, the use of Bagley corrections in predicting wall shear stresses in blends is invalid. The data presented from this point on are not corrected for entrance pressure effects.

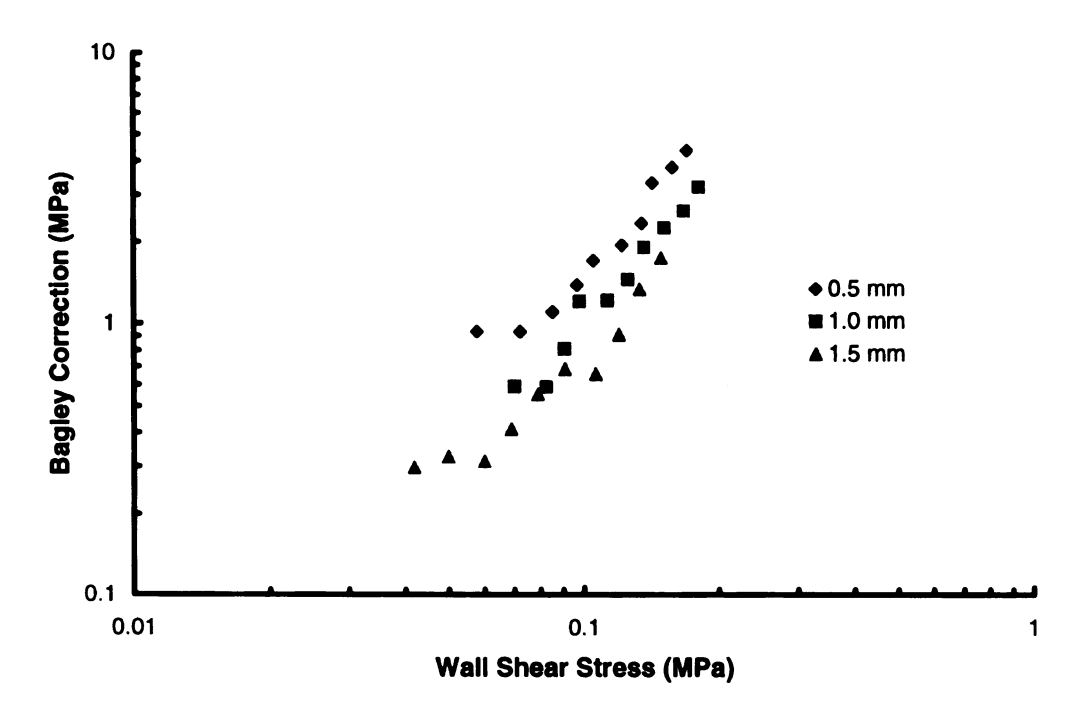


Figure 4.7 Bagley corrections for 80/20 6323 PP/MDE 251 at 200°C.

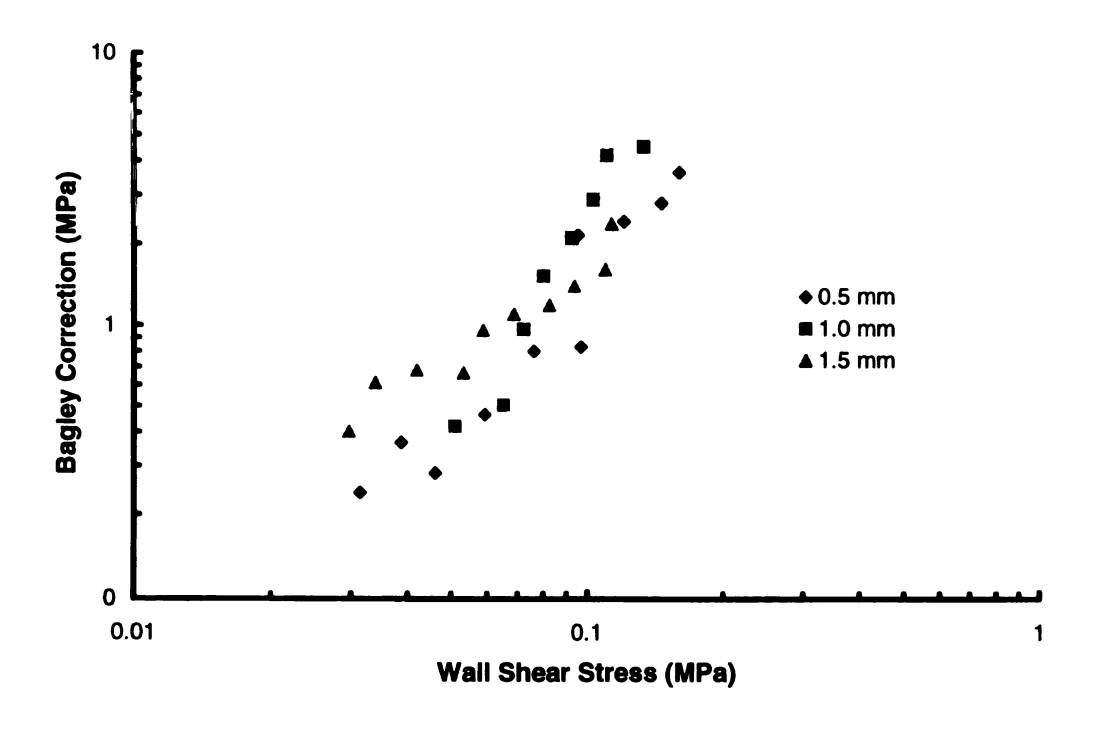


Figure 4.8 Bagley corrections for 80/20 6323 PP/CO-043 at 200°C.

### 4.5.2 Mooney analysis

Although the Mooney plot can not be used in this case to infer slip, re-plotting the uncorrected data on Mooney coordinates can provide some insight as to how the morphology is changing with respect to die diameter and apparent shear rate. The main changes in morphology that are expected to occur are migration and stretching of the rubber drops. Before proceeding, it is useful to define mean residence time, which is represented as

$$\frac{L}{\overline{u}} = \frac{8\frac{L}{D}}{\dot{\gamma}_{app}} \tag{4-1}$$

where L is the length of the die, D is the diameter of the die,  $\overline{u}$  is the mean velocity, and  $\dot{\gamma}_{app}$  is the apparent shear rate. Plotting the mean residence time versus wall shear stress (Figure 4.9) shows that the residence times are lowest for the smallest L/D and that for a given L/D, the smallest diameter has the longest resident time. As residence time varies inversely with shear rate, less migration is expected to occur at high shear rates than at low shear rates. In terms of stretching, high shear rates lead to more elongation, especially in the smaller diameter dies.

Figures 4.10 and 4.11 show the Mooney plots for L/D=20 of the uncorrected MDE 251 and CO-043 blend data. The trends between the blends are similar as both plots show the same type and degree of curvature, even though the MDE 251 was found to have a wider drop size distribution than the CO-043 (Figures 3.2 and 3.3). The progression of increasing apparent viscosity (decreasing apparent shear rate) with decreasing die diameter suggests that apparent slip in both blends *increases* with diameter. As shown in Chapter 3, the wall region in all of the CO-043 extrudates showed

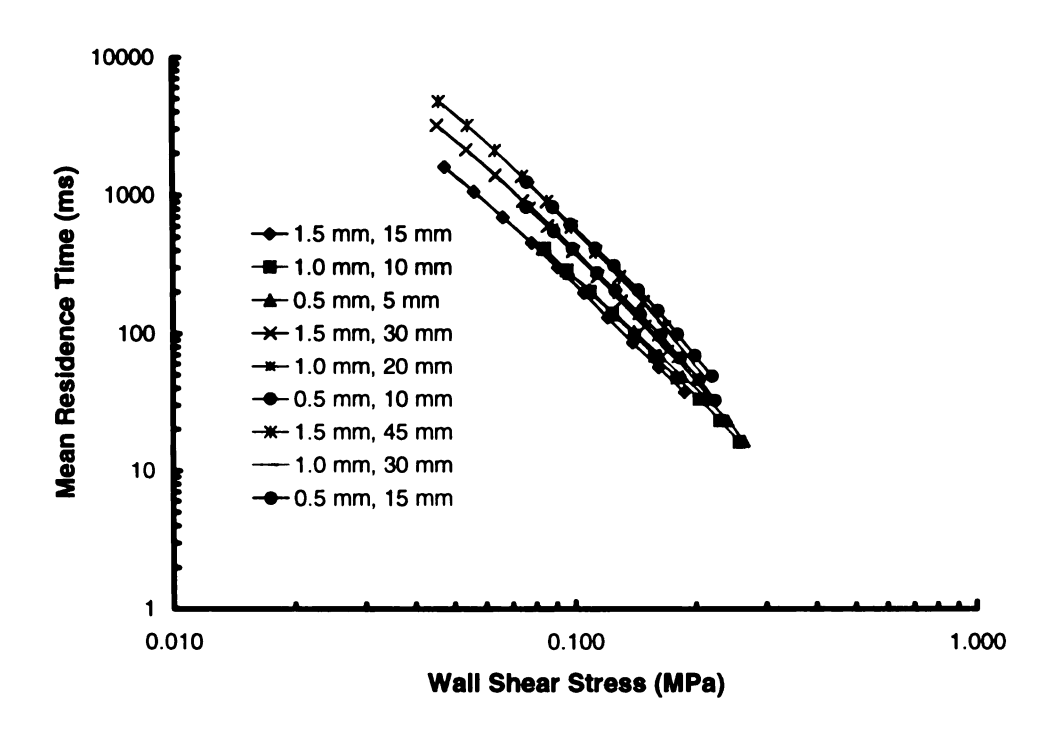


Figure 4.9 Mean residence time versus wall shear stress for various die geometries.

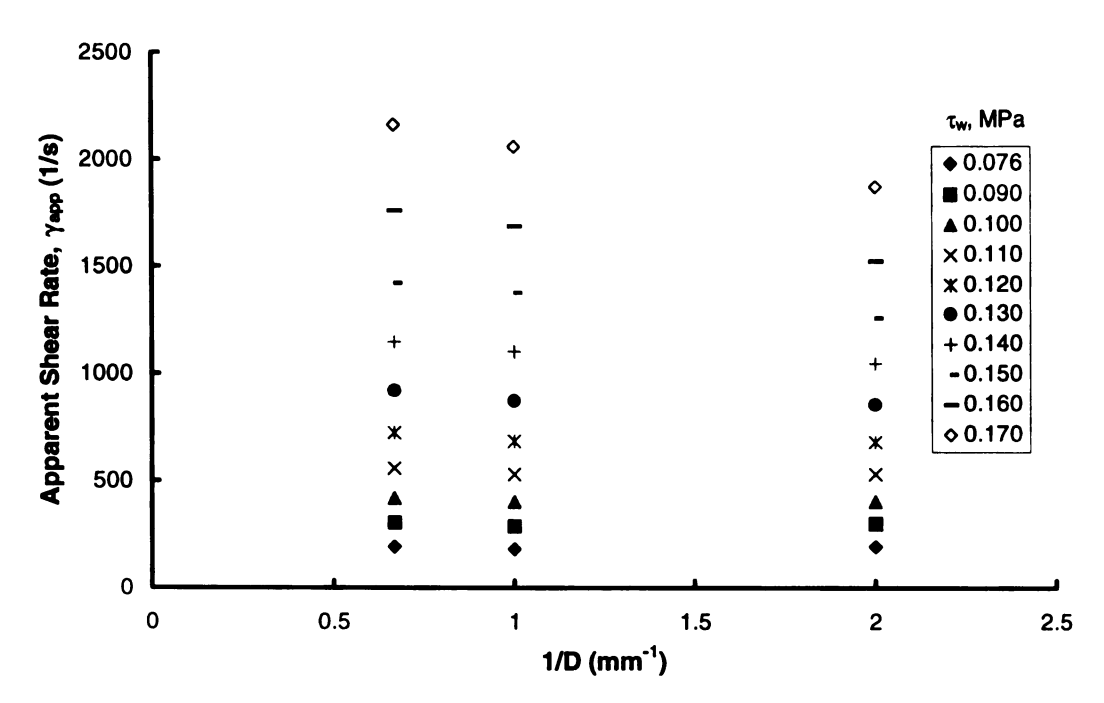


Figure 4.10 Mooney plot for 80/20 6323 PP/MDE 251 at 200°C, L/D=20.

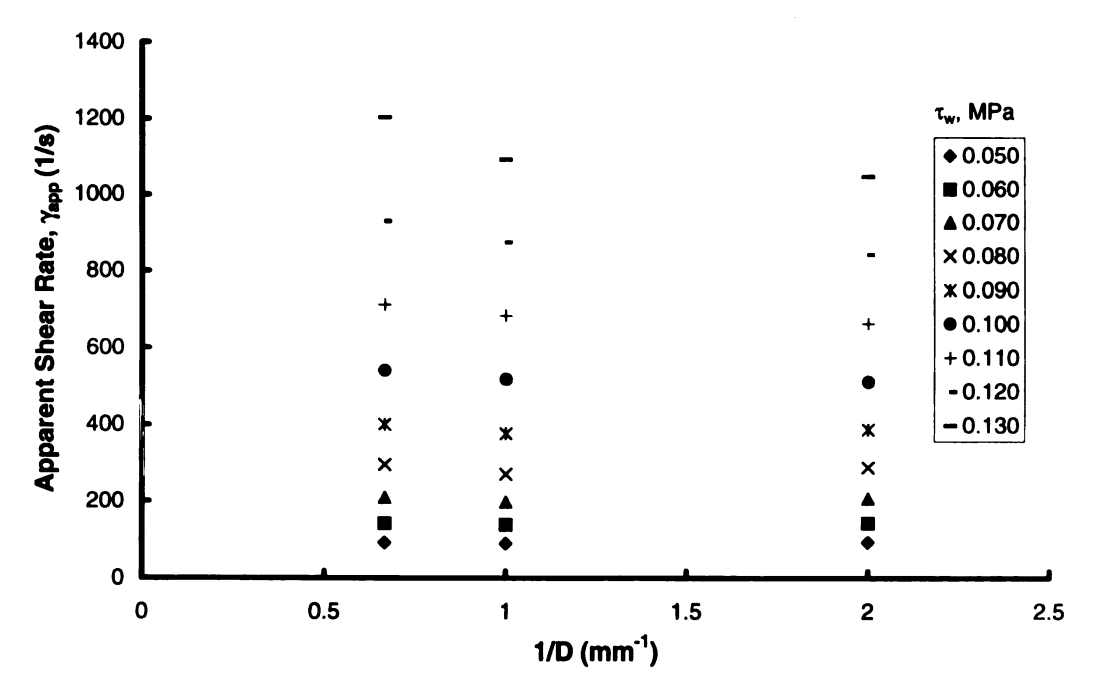


Figure 4.11 Mooney plot for 80/20 6323 PP/CO-043 at 200°C, L/D=20.

a depletion of rubber drops. Migration of the rubber drops is believed to occur more readily in the large-diameter dies than in the small-diameter dies, especially at high shear rates, since more stretching is expected to occur in the small diameter die.

From the work of Phillips *et al.* (1992), who developed a constitutive equation for concentrated suspensions that undergo shear-induced migration, it has been shown that there are two main mechanisms for particle flux in these systems. These are the particle fluxes due to the collision frequency and the viscosity gradient, which are denoted as  $N_c$  and  $N_{\eta}$  respectively. The expressions for the fluxes are given as

$$N_c = -K_c a^2 \phi \frac{\partial}{\partial r} (\phi \dot{\gamma}) \tag{4-2}$$

$$N_{\eta} = -K_{\eta} \frac{a^2 \dot{\gamma} \phi^2}{\eta} \frac{d\eta}{dr} \tag{4-3}$$

where a is the particle radius,  $\phi$  is the volume fraction,  $\eta$  is the suspension viscosity, and  $\dot{\gamma}$  is the shear rate. The constants  $K_c$  and  $K_{\eta}$  are the model parameters determined from experiment. The flux due to collisions  $N_c$  is in the direction of decreasing shear rate, so that drop migration is driven towards the center, shear-free zone of the die, while the flux due to the viscosity gradient  $N_{\eta}$  is in the opposite direction, so that the drops are driven to regions of lower viscosity (i.e. the wall).

The suspension viscosity,  $\eta$ , depends not only on the drop concentration, but is also a function of drop aspect ratio. Stretching at the core is expected to occur to a greater degree in the small diameter die, since the large contraction ratio yields more extensional flow. The flux due to the viscosity gradient will be significantly greater than

the flux due to collisions in small diameter dies as compared to large diameter dies. This translates to an overall lesser migration of the drops from the wall to the core in small diameter dies, so that the maximum rubber concentration lies closer to the wall in a small diameter die than in a large diameter die (Figure 4.11). Less migration means less depletion of rubber from the wall layer and thus a higher apparent viscosity (i.e., less apparent slip).

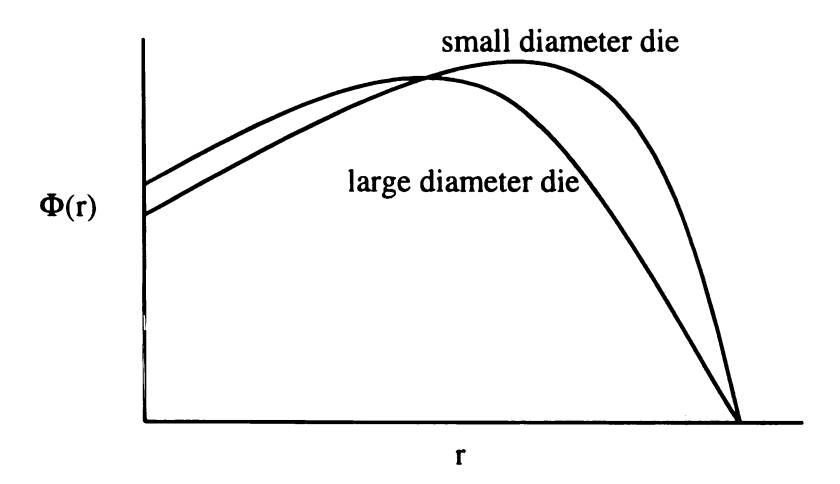


Figure 4.12 Schematic of dispersed phase concentration variation over radial position.

#### 4.5.3 Recoverable strain in blends

Extrudate swell is the response of a polymer melt to recover strain and return to its original shape on emergence from the capillary. Data on the extrudate swell of 6323 PP and the 80/20 PP/EP blends was converted to recoverable strain as follows

Recoverable strain = 
$$\left(\frac{d}{D}\right)^2 - 1$$
 (4-5)

where the d is the diameter of the extrudate as it exits a die of diameter, D.

As seen in the plot of recoverable strain versus wall shear stress (Figure 4.12), the blends have a characteristically lower extrudate swell than the 6323 PP. Newman and Trementozzi (1965) conducted a study on the influence of fillers on extrudate swell in poly(styrene-acrylonitrile) and found that the extrudate swell in these systems decreased with increased filler content. The presence of filler was also found to increase the tendency for plug flow by developing a region of low filler concentration at the surface, causing a significant reduction in the local viscosity from that of the interior, and also by the "trapping" of the matrix polymer. The more stretched the rubber drops, the more constrained the matrix, so that less material is able to recover from the imposed strain.

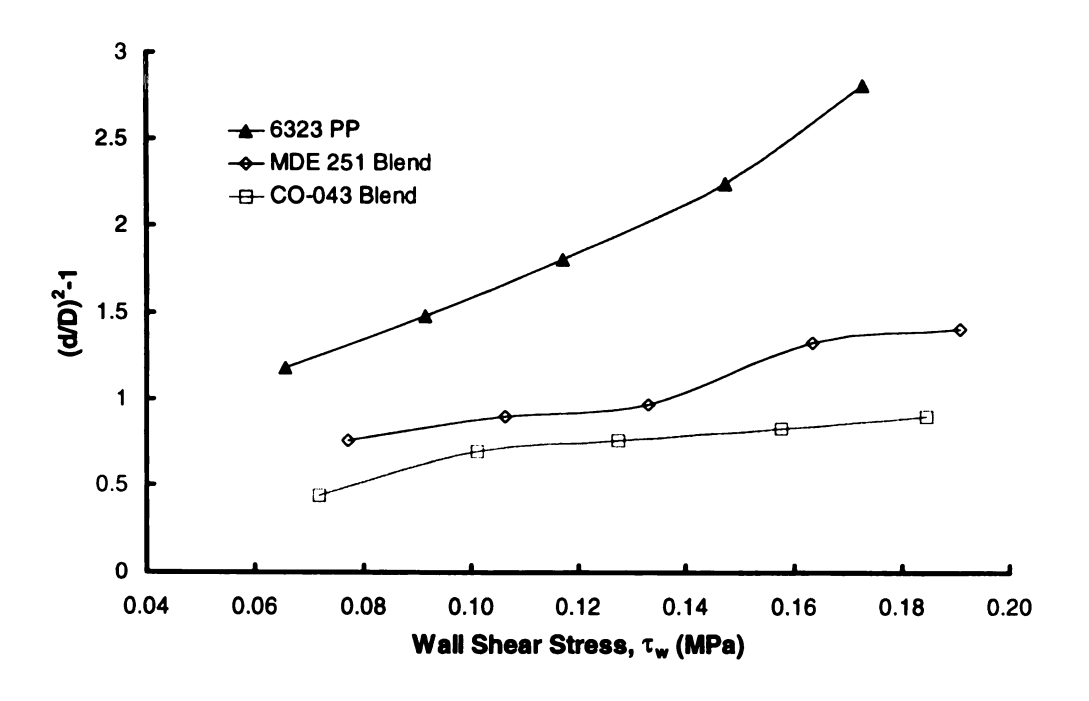


Figure 4.12 Recoverable strain for 80/20 PP/EP blends at 200°C, L/D =30, D= 1 mm.

### **4.6 Conclusions**

The Bagley plots for neat polypropylene and the two blends were found to be slightly curved, and were thus fitted with a second-order polynomial in determining the ends correction. For neat polypropylene and the blend containing MDE 251, the Bagley correction was found to depend on contraction ratio; however, for the CO-043 blend, the Bagley correction did not follow any consistent trend with diameter.

An estimate of the slip velocity for neat polypropylene showed that slip velocity decreased with increasing L/D, presumably because of the increasing effect of pressure. For the blends, Mooney plots of the *uncorrected* data showed a reverse trend in slip velocity with diameter, as the large diameters exhibited more slip than the smaller die diameters. Greater apparent slip was found in the larger diameters, where more migration is expected to occur. The amount of migration that occurs is explained in the terms of two competing fluxes, the flux due to viscosity variations and the flux due to collision. As viscosity depends on the aspect ratio of the drops, the flux due to viscosity is expected to be significantly greater than the flux due to collisions in a small diameter die, where more stretching is expected to occur. This leads to a higher viscosity barrier in the core region for migration, so that less migration occurs in the small diameter.

The recoverable strain of the blends were found to be considerably lower than that of neat PP. The reduction in the recoverable strain of the blends is attributed to the reduction in the local viscosity in the wall layer due to migration of the rubber drops, and by the constraining of the matrix by the stretched rubber drops.

#### CHAPTER 5

#### CONCLUSIONS AND RECOMMENDATIONS

#### **5.1 Conclusions**

In the extrusion of blends containing polypropylene and EP rubber, the following trends in morphology were observed:

- Migration of large rubber drops from the wall to the core leading to a depletion in the wall region.
- 2. Maximum stretching of the drops at the center or shear-free zone of the die, due mainly to the normal stress differences between the rubber and the matrix. This is in contrast with what Bousmina and Muller (1996) found in their study of PMMA/rubber blends that the greatest stretching occurred in the wall region.
- 3. Stretching in the wall region along the vorticity direction.

Flow tests conducted on neat polypropylene showed that the Bagley corrections increased with increasing contraction ratio. The slight curvature in the Bagley plot was attributed to the pressure dependence of slip velocity, which decreased with increasing L/D. Curvature observed in the Mooney chart was also attributed to the pressure dependence of slip velocity and to possible viscous heating effects.

In the MDE 251 blend, the Bagley corrections were found to increase with increasing contraction ratio; however, no discernible trend was found to occur in the blend containing CO-043. Mooney plots of the uncorrected data for the blends showed that greater apparent slip occurred in the larger diameter die, suggesting that migration

occurs more readily in the larger diameter die. This can be explained in terms of  $N_c$  and  $N_{\eta}$ , the fluxes due to collision between the EP rubber drops and the viscosity gradients, respectively. In the smaller diameter die, more stretching at the center is expected to occur, since the large contraction ratio yields more extensional flow. Since viscosity increases with aspect ratio, there is a greater viscosity barrier for migration in the small diameter die.

#### **5.2 Recommendations for Further Work**

The ultimate goal of this research is to come up with a model which relates trends in rheology to trends in morphology in these blends. To do so, requires a comphrensive understanding of how the morphology changes under different conditions (i.e., die diameter, shear rate, etc.). Further work should focus on obtaining a more detailed picture of the drop deformation and migration under different conditions.



### **APPENDIX A**

#### **IMAGE ANALYSIS**

#### A.1 Determination of Area Fraction

The SEM micrographs were scanned into JPEG image files and analyzed using Sigma Scan 3.0 from Jandel Scientific. The areas of the voids left from dissolution of the EP rubber were determined by one of two methods. In regions 1 & 2 (Figure 3.3 and Table 3.3), where the voids were relatively circular, the diameters of the voids were measured and the areas were determined by

Area of Void 
$$i = A_i = \frac{\pi D^2}{4}$$

For region 3 and the flow plane micrographs for sample E (Figure 3.3 and Table 3.3), where the voids took an irregular shape, the actual areas were measured using the software. After a sufficient number, n, of voids were counted ( $\geq 800$ ), the total area occupied by the measured voids,  $A_{tot}$ , was determined and the area fraction of the CO-043 rubber phase was calculated by

Total Area Fraction = 
$$\frac{\sum_{i=1}^{n} \frac{A_i}{A_{tot}}}{A_{tot}}$$

### A.2 Determination of Average Aspect Ratio, $\ell$

A feature in Sigma Scan 3.0 allows measurement of the major and minor axis lengths of object areas. The major axis is defined by searching all the border pixels of an object and choosing the two pixels that are the farthest apart. Once a major axis is

defined, the minor axis can be calculated. Minor axes are drawn between two pixels defining the longest line perpendicular to the major axis. The aspect ratio for a void is then calculated by

$$\ell_i = \left(\frac{\text{major axis length}}{\text{minor axis length}}\right)_i$$

The average aspect ratio is then determined by

$$\ell_{v} = \sum_{i=1}^{n} \ell_{i} \left( \frac{A_{i}}{A_{tot}} \right)$$

### APPENDIX B

#### **DETERMINATION OF VOLUME FRACTION**

The volume fraction is related to the area fraction by some factor a, or

$$\phi = \frac{\sum_{j=1}^{n} n_{j} A_{j}}{A_{cor}} \times a$$

To determine a, one must solve the relevant mass balance for flow through a capillary. For a capillary of radius R, the integral mass balance written in terms of volume fraction  $\phi(r)$  is

$$\frac{2}{R^2}\int_{0}^{R}v(r)\phi(r)rdr=\overline{v}\overline{\phi}$$

where v(r) is the velocity profile,  $\overline{v}$  is the mean velocity, and  $\overline{\phi}$  is the bulk volume fraction. The volume fraction can be written in terms of area fraction as

$$\phi(r) = a\phi_A(r)$$

Substitution of this expression into the mass balance, yields

$$\frac{2a}{R^2}\int_{0}^{R}v(r)\phi_{A}(r)rdr=\overline{v}\,\overline{\phi}$$

To non-dimensionalize, we let

$$\zeta = \frac{r}{R}$$

Re-writing the mass balance in non-dimensional form and solving for a gives

$$2a\int_{0}^{1} \frac{v(\zeta)}{\overline{v}} \phi_{A}(\zeta) \zeta d\zeta = \overline{\phi} \Rightarrow a = \frac{\overline{\phi}}{2\int_{0}^{1} \frac{v(\zeta)}{\overline{v}} \phi_{A}(\zeta) \zeta d\zeta}$$

For plug-flow,  $\frac{v(\zeta)}{\overline{v}} = 1$  so that

$$a = \frac{\overline{\phi}}{2\int_{0}^{1} \phi_{A}(\zeta) \zeta d\zeta}$$

For non-plug flow through a long tube, the velocity profile cannot be assumed to be 1. The velocity profile  $u_z(r)$  and volumetric flow rate Q for a power law fluid are given as (Middleman, 1977)

$$u_{z}(r) = \frac{nR}{1+n} \left(\frac{R\Delta P}{2KL}\right)^{1/n} \left[1 - \left(\frac{r}{R}\right)^{1+1/n}\right]$$

$$Q = \frac{n\pi R^3}{1+3n} \left(\frac{R\Delta P}{2KL}\right)^{1/n}$$

The mean velocity is determined from

$$\overline{u} = \frac{Q}{\pi R^2} = \frac{nR}{1 + 3n} \left( \frac{R\Delta P}{2KL} \right)^{1/n}$$

Dividing the velocity profile by the mean velocity yields

$$\frac{u_z}{\overline{u}} = \left(\frac{1+3n}{1+n}\right)\left[1-\left(\frac{r}{R}\right)^{1+1/n}\right]$$

The value of a was determined for both plug and normal flow. For normal flow, the value of n was set to 0.33, the value for 6323 polypropylene. The values of a for normal and plug flow were 1.26 and 1.31, respectively. Since plug flow has been shown to occur in filled systems (see Chapter 2), the plug flow value for a was used in determination of volume fraction.



# **Bibliography**

- 1. Arp, P.A. and S.G. Mason, J. Colloid Interface Sci., 61, 44-61 (1977).
- 2. Benbow, J.J., R.N. Charley, and P. Lamb, Nature, 192, p.223 (1961).
- 3. Bousmina, M. and R. Muller, *Rheol. Acta*, **35** (4), 369-381 (1996).
- 4. Chan, C.-M. and J. Feng, J. Rheol., 41 (2), 319 (1997).
- 5. Chang, M.C.O., SPE Tech Papers, 40, p.36 (1994).
- 6. Denn, M.M., Ann. Rev. Fluid Mech., 22, 13-34 (1990).
- 7. Denn, M.M., *Theoretical and Applied Rheology*, eds. P. Moldenaers and R. Keunings, p. 45-49 (1992).
- 8. El Kissi, N. and J.M. Piau, J. Non-Newt. Fluid Mech., 37, 55-94 (1990).
- 9. Geiger, K., Kautsch und Gummi Kunstst B, 19 (7), 507 (1989).
- 10. Grace, H.P., Chem. Eng. Commun., 14, 225-277 (1982).
- 11. Graham, A.L., A.A. Mammoli, and M.B. Busch, *Rheol. Acta*, 37 (2), 139-150 (1998).
- 12. Hamada, H. and H. Tsunasawa, J. App. Polym. Sci., 60 (3), 353-362 (1996).
- 13. Hampton, R.E., A.A. Mammoli, A.L. Graham, N. Tetlow, and S.A. Altobelli, J. *Rheol.*, 41 (3), 621-640 (1997).
- 14. Han, C.Y., M.D. Wolkowicz, D. Dong, and S.S. Dagli, SPE Tech Papers, 42, (1996).
- 15. Han, J.H., C.C.-Feng, D.-J. Li, and C.D. Han, *Polymer*, **36** (12), 2451-2462 (1995).
- 16. Hatzikiriakos, S.G. and J.M. Dealy, J. Rheol., **35** (4), 497-523 (1991).
- 17. Hatzikiriakos, S.G. and J.M. Dealy, J. Rheol., **36** (4), 703-741 (1992).
- 18. Hatzikiriakos, S.G. and J.M. Dealy, *Polym. Eng. Sci.*, **34** (6), 493-499 (1994).
- 19. Hobbie, E.K. and K.B. Migler, *Phys. Rev. Letters*, **82** (26), 5393-5396 (1999).
- 20. Hobbs, S.Y., *Polym. Eng. Sci.*, **36** (11), 1489-94 (1996).
- 21. Karam, H.J. and J.C. Bellinger, *Ind. Eng. Chem. Fundam.*, 7, 576-581 (1966).

- 22. Karnis, A., H.L. Goldsmith, and S.G. Mason, J. Colloid Interface Sci., 22, 531-533 (1966).
- 23. Kazatchkov, I.B., S.G. Hatzikiriakos, and C. Stewart, *Polym. Eng. Sci.*, **35** (23), 1864-1871 (1995).
- 24. Koh, C.J., P. Hookman, and L.G. Leal, J. Fluid Mech., 266, 1-32 (1994).
- 25. Laun, H.M. and H. Schuch, J. Rheol., 33, 119 (1990).
- 26. Laun, H.M., Rheol. Acta, 22, 171 (1983).
- 27. Leighton, D.T. and A. Acrivos. J. Fluid Mechanics, 181, 415-439 (1987).
- 28. Levitt, L., C.W. Macosko, S.D. Pearson, *Polym Eng. Sci.*, **36** (12), 1647 (1996).
- 29. Macosko, C.W., Rheology: Principles, Measurements, and Applications, VCH, New York, 1994.
- 30. Majors, P.D., A.L. Graham, and M. Gottlieb, *Proc. 10th Intl. Congr. Rheology*, *Sydney, Australia*, **2**, 137-139 (1988).
- 31. Malkin, A. Ya, A.V. Baranov, and M.E. Vikulenkova, *Rheol. Acta*, **32** (2), 150-155 (1993).
- 32. Middleman, S., Fundamentals of Polymer Processing, p. 88 (1977).
- 33. Mighri, F., A. Ajji, P.J. Carreau, J. Rheol., 41: (5) 1183-1201 (1997).
- 34. Mooney, M., J. Rheol., 2, 210 (1931).
- 35. Mourniac, Ph., J.F. Agassant and B. Vergnes, *Rheol. Acta*, 31 (6), 565-574 (1992).
- 36. Newman, S. and Trementozzi, Q.A., J. App. Polym. Sci., 9, 3071-3089 (1965).
- 37. Phillips, R.J., R.C. Armstrong, and R.A. Brown, *J. Non-Newt. Fluid Mech.*, **64**, 157-171 (1996).
- 38. Rofe, C.J., L. de Vargas, J.P.-Gonzalez, R.K. Lambert, and P.T. Callaghan, *J. Rheol.*, **40** (6), 1115-1128 (1996).
- 39. Rosenbaum, E.E., and S.G. Hatzikiriakos, *AIChE J.*, **43** (3), 598 (1997).
- 40. Schowalter, W.R., J. Non-Newt. Fluid Mech., 29 (1-3), 25-36 (1988).
- 41. Shidara, H. and M.M. Denn, J. Non-Newt. Fluid Mech., 48 (1-2), 101-110 (1993).
- 42. Sinton, S.W. and A.W. Chow, *J. Rheol.*, **35**, 735-772 (1991).

- 43. Torza, S., R.G. Cox, and S.G. Mason, J. Colloid Interface Sci., 38, 395-411 (1972).
- 44. Vinogradov, G.V. and L.I. Ivanova, Rheol. Acta, 6 (3), 209-222 (1967).
- 45. White, J.L., M.H. Han, N. Nakajima, and R. Brzoskowski, J. Rheol., 35 (1), 167-189 (1991).